AD-A085 148 NAVAL POSTGRADUATE SCHOOL MONTEREY CA F/G 13/10
ANALYSIS OF JET-CROSSFLOW INTERACTIONS WITH APPLICATION TO SHIP--ETC(U)
MAR 80 B B WATERMAN

UNCLASSIFIED NL

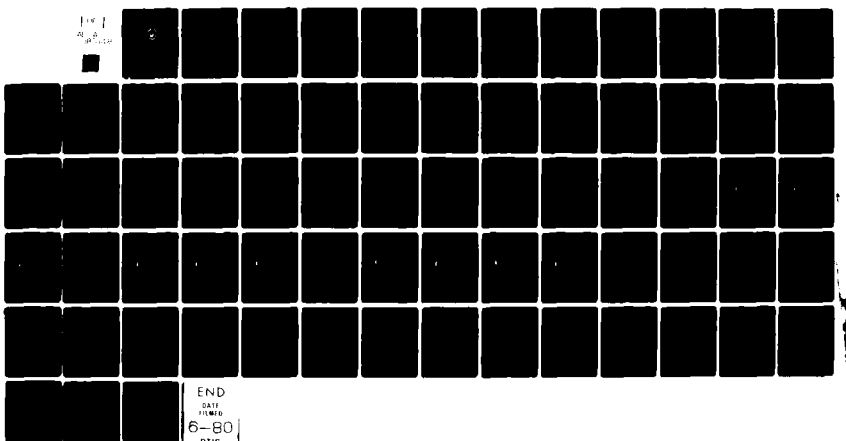

END
DATE FILMED
6-80
DTIC

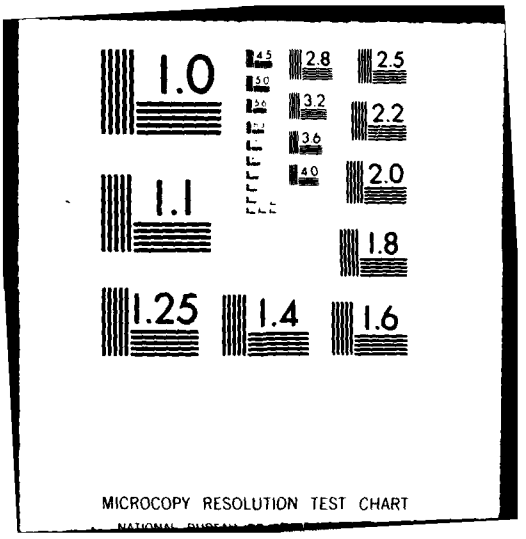
1.0
1.1
1.25
1.4
1.6
1.8
2.0
2.2
2.5
2.8
3.2
3.6
4.0
4.5
5.0
MICROCOPY RESOLUTION TEST CHART

NAVAL POSTGRADUATE SCHOOL
Monterey, California

THESIS

ANALYSIS OF JET-CROSSFLOW INTERACTIONS
WITH APPLICATION TO SHIP BOW THRUSTERS

by

Bradford Bates Waterman, III

March 1980

Thesis Advisor: R. H. Nunn

Unclassified

SECURITY CLASSIFICATION OF THIS PAGE (When Data Entered)

REPORT DOCUMENTATION PAGE	READ INSTRUCTIONS BEFORE COMPLETING FORM
1. REPORT NUMBER	2. GOVT ACCESSION NO. AD-A085 148 / 3. RECIPIENT'S CATALOG NUMBER (9)
4. TITLE (and Subtitle) (6) Analysis of Jet-Crossflow Interactions With Application to Ship Bow Thrusters.	5. TYPE OF REPORT & PERIOD COVERED Master's Thesis March 1980 / 6. PERFORMING ORG. REPORT NUMBER
7. AUTHOR(s) (10) Bradford Bates Waterman, III	8. CONTRACT OR GRANT NUMBER(s)
9. PERFORMING ORGANIZATION NAME AND ADDRESS Naval Postgraduate School Monterey California 93940	10. PROGRAM ELEMENT, PROJECT, TASK AREA & WORK UNIT NUMBERS
11. CONTROLLING OFFICE NAME AND ADDRESS Naval Postgraduate School Monterey, California 93940 (11)	12. REPORT DATE March 1980 / 13. NUMBER OF PAGES 70
14. MONITORING AGENCY NAME & ADDRESS(if different from Controlling Office) (12) 71	15. SECURITY CLASS. (of this report) Unclassified / 15a. DECLASSIFICATION/DOWNGRADING SCHEDULE

16. DISTRIBUTION STATEMENT (of this Report)

Approved for public release; distribution unlimited.

17. DISTRIBUTION STATEMENT (of the abstract entered in Block 20, if different from Report)

18. SUPPLEMENTARY NOTES

19. KEY WORDS (Continue on reverse side if necessary and identify by block number)

Bow Thrusters
Jets/Crossflows

20. ABSTRACT (Continue on reverse side if necessary and identify by block number)

An analytical model of a jet injected normally from a flat plate into a uniform crossing flow was formulated to provide a simplified method of predicting the interference effects arising from the complex flow fields induced by ship bow thrusters. This model was an extension of previous work based upon a description of the jet as a series of distributed vortices. The analysis takes into account the position of the effective source of the jet and the blockage due to the presence of the jet in the

DD FORM 1 JAN 73 1473 (Page 1) EDITION OF 1 NOV 68 IS OBSOLETE S/N 0102-014-6601

Unclassified

SECURITY CLASSIFICATION OF THIS PAGE (When Data Entered)

251450 (13)

Block 20 continued...

crossflow. For representative jet-to-crossflow velocity ratios, the flow field and pressure distributions were calculated utilizing different combinations of effective source position and blockage. The accuracy of the model was evaluated by comparison with the available experimental data. Although good agreement was achieved for large portions of the interaction field, several regions were identified requiring further analytical description.

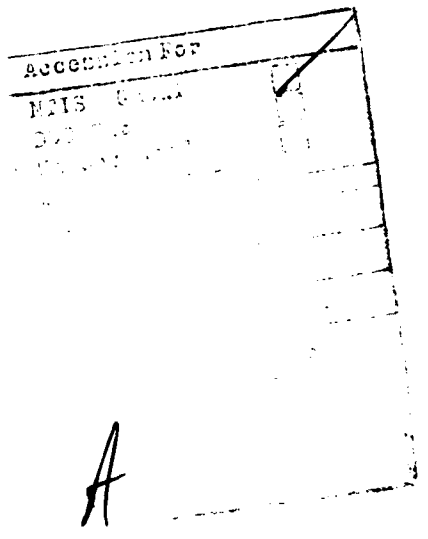

Approved for public release; distribution unlimited

Analysis Of Jet-Crossflow Interactions With Application To Ship Bow Thrusters

by

Bradford Bates Waterman, III
Lieutenant Commander, United States Navy
B.S., Tufts University, 1968

Submitted in partial fulfillment of the requirements for the degree of

MASTER OF SCIENCE IN MECHANICAL ENGINEERING

and

MECHANICAL ENGINEER

FROM THE

NAVAL POSTGRADUATE SCHOOL
March 1980

Author Bradford B. Waterman III

Approved by: _____
Thesis Advisor

_____
Chairman, Department Of Mechanical Engineering

_____
Dean Of Science And Engineering

ABSTRACT

An analytical model of a jet injected normally from a flat plate into a uniform crossing flow was formulated to provide a simplified method of predicting the interference effects arising from the complex flow fields induced by ship bow thrusters. This model was an extension of previous work based upon a description of the jet as a series of distributed vortices. The analysis takes into account the position of the effective source of the jet and the blockage due to the presence of the jet in the crossflow. For representative jet-to-crossflow velocity ratios, the flow field and pressure distributions were calculated utilizing different combinations of effective source position and blockage. The accuracy of the model was evaluated by comparison with the available experimental data. Although good agreement was achieved for large portions of the interaction field, several regions were identified requiring further analytical description.

TABLE OF CONTENTS

LIST OF FIGURES

ACKNOWLEDGEMENT

The author wishes to express his appreciation to Associate Professor Robert Nunn for his advice and guidance during the development of this model. Without his valuable assistance, this could not have been completed.

Many thanks to my wife, Helga, for her infinite understanding and patience during the long hours needed for its completion.

I. INTRODUCTION

In recent years there has been an increase in the installation and use of hull mounted, tunneled bow thrusters to improve ship maneuverability in restricted situations, such as dynamic position holding and confined waters docking. This increase has created renewed interest in the development of an ability to predict bow thruster performance. To date, there has been relatively little pre-installation design consideration regarding precise power requirements or ultimate operational performance. The limited testing that has been conducted [1-4]* has resulted in a recurring major problem, namely, radical variations in effective turning moment with minor changes in ship speed. Chislett and Bjorheden [4] noted that "an area of low pressure is created downstream of the discharging jet producing a resultant suction force that has a shifting center of action with changes in ship speed," thereby altering the effective moment produced by the thruster. The ability to predict the magnitude of this resultant suction force and its center of action would permit designers to accurately determine powering and control requirements for thrusters.

This problem of radical variations in effective side forces and turning moments with only minor changes in ship speed may be better understood by considering the general

*Numbers in brackets refer to references listed.

equations of motion of a ship moving in the horizontal plane of the sea. From [5] these equations are:

$$m(\dot{u} - rv) = X$$

$$m(\dot{v} - ru) = Y$$

$$I_z\dot{r} = N$$

where m = mass of the ship

u = velocity in the x-direction

v = velocity in the y-direction

r = angular velocity

I = mass moment of inertia

X = excitation force(s) in x-direction

Y = excitation force(s) in y-direction

N = excitation torque(s)

(dots indicate differentiation with respect to time)

To minimize the complexity of the following brief analysis, all forces and torques will be referred to the ship's center of gravity. See Fig. 1.

When these equations are transformed into their linearized version [5], they become

$$- X_u(u - u_o) + (m - X_{\dot{u}})\, u_o = X$$

$$- Y_v v + (m - Y_{\dot{v}})\dot{v} - (Y_r - mu_o)r - Y_{\dot{r}}\dot{r} = Y$$

$$- N_v v - N_{\dot{v}}\dot{v} - N_r r + (I_z - N_{\dot{r}})\dot{r} = N$$

where the subscripts u, $\dot{u}$, v, $\dot{v}$, r, $\dot{r}$, denote differentiation with respect to the variable subscripts, and u_o is constant reference surge velocity. The left sides of these equations explicitly represent the velocity and acceleration dependent

reactions due to drag, added mass, added inertia and other coupled motions; while the right sides implicitly represent excitation force(s) and moment(s), which are in this analysis due to the thruster. Since this is a linearized formulation utilizing small angle perturbations, the excitation force in the x-direction is negligible compared to that in the y-direction:

$$X << Y$$

therefore X≈0. The y-direction excitation force can be expressed as

$$Y = Y_j + Y_i \tag{1}$$

where $Y_j = \dot{m}_j U_j$, the ideal jet thrust produced by the thruster, and Y_i is the induced force created by the interaction of the thruster discharge with the flow past the ship. Utilizing experimental data from [4] in the range, $0.1 \leq \frac{U}{U_j} \leq 0.25$, Y_i can be approximated by a linear function of ship speed

$$\frac{Y_i}{Y_j} = 0.22 + k\left(\frac{U}{U_j}\right) \tag{2}$$

where $-3.0 < k < -1.5$. Substituting a nominal value of $k = -2.0$ and $Y_j = \dot{m}_j U_j$ into equation (2) gives

$$Y_i = \dot{m}_j U_j \left[0.22 - 2.0 \left(\frac{U}{U_j}\right)\right] \tag{3}$$

Substituting equation (3) into equation (1) results in

$$Y = \dot{m}_j U_j \left[1.22 - 2.0\left(\frac{U}{U_j}\right)\right]$$

which explicitly couples the y-direction motion to the x-direction motion, normally uncoupled in the linear approximation. In addition to the coupling, in the relevant velocity ratio range, $0.1 < \frac{U}{U_j} < 0.25$, there is an appreciable reduction in the net thruster force due to motion in the x-direction. Furthermore, the moment produced by the thruster is a function of the net effective thrust, Y, and a characteristic moment arm, x_t:

$$N_t = x_t Y$$

As reported by Refs. [1-3], the degradation of net effective thrust is accompanied by a shift in the center of action of the induced force, Y_i, which results in a change in the characteristic moment arm. This shift in the thruster's net effective thrust center of action is a direct consequence of the coupling of x-direction motion with turning moment.

This simplified analysis, which neglected all excitations other than the thruster, points out the complex, coupled motions arising from the interaction of the thruster discharge and the flow past the ship. To fully understand this highly non-linear, three-dimensional flow situation extensive analytical and experimental work is required. This thesis will attempt to provide some understanding of the interaction of a jet discharging into a uniform cross-flow in order to develop some ability to predict the degradation of net effective thrust.

II. BACKGROUND

A survey of the literature pertaining to the installation and operation of bow thrusters revealed a surprising lack of experimental data, considering the number of units currently installed. English [1,2], Stuntz and Taylor [3], and Chislett and Bjorheden [4] present some data from model tests conducted at various facilities, but in these works there is no formalized recording of full scale test or actual installation test data. However, further investigation led to a related field: Vertical or Short Take-Off and Landing Aircraft (V/STOL) research. The concept of using air jets positioned in aircraft wings to provide vertical take-off and landing capability correlates extremely well with flow patterns produced by a bow thruster. As reported by Bradbury and Wood [6] for incompressible flow, the jet (thruster discharge) path and induced flow are dependent mainly on the momentum flux ratio, $\rho_j U_j^2/\rho U^2$, and independent of Reynolds number. Margason [7] and Gordier [8] also reported that the effective velocity ratio is the predominate characteristic in determining the path of the jet. Therefore, until more extensive ship or model data have been collected, the results of V/STOL research are used as a basis for predictive theories.

Although there has been a good deal of research conducted in the area of air jets in cross-flows, the majority of the work has been concerned with analytically or empirically

defining the jet trajectory and jet cross-section geometry. The interference effects of the interacting flows have received relatively little attention. A fluid jet injected into a crossing stream has previously been described as a turbulent, three-dimensional, highly non-linear flow problem which, even with considerable simplification, requires extensive computer time to numerically solve the appropriate form of the Navier-Stokes equations [9]. Therefore, early investigators have sought simplified methods for determining the interaction effects, such as pressure and velocity distributions, and have realized the necessity of knowing the geometry of the jet: trajectory and shape.

Experimental data form the basis for most trajectory formulations. Either pressure or velocity measurements have been taken in the flow field encompassing the jet-crossflow interaction region and curves fit through points of maximum pressure or velocity. These curves were then compared with flow visualizations. In some instances, semi-empirical formulations were derived from the conservation laws combined with experimentally determined constants. Abramovich [10] qualitatively described the turbulent jet in a deflecting flow and presented some empirical methods for predicting the trajectory of the deflected jet. Jordinson [11] presented trajectory data by recording and plotting contours of total pressure coefficients. Keffer and Baines [12] presented experimental results from which it was determined that for various jet strengths, the jet trajectories could

be represented by a single function. Gordier [8], the only reported source of water jet-water crossflow experiments, presented an empirical jet trajectory formulation based on a curve passed through experimental points of maximum total pressure. Sucec and Bowley [9] formulated an analytical expression for the jet trajectory utilizing previous experimental information and the assumption that the distributed pressure force and entrained momentum flux could be approximated by an aerodynamic drag force. Margason [7] utilized flow visualization techniques and pressure measurements to formulate a trajectory equation. In addition, his paper also reviewed and compared the results of a number of other studies concerned with trajectory prediction. All the above predictive formulations produced trajectories within a range of uncertainty that can be attributed to expected experimental error, differences in test procedures and facilities, and in the case of analytical formulations, simplifying assumptions. In view of this, it was concluded that any one of them reflected the current state of the art in trajectory prediction.

The ability to predict the jet trajectory is of definite importance, but the primary objective of this jet-crossflow research is to provide insight into the changes, in the otherwise uniform flow, created by injecting a jet. Experiments conducted by Bradbury and Wood [6], Vogler [13], Fearn and Weston [14], McMahon and Mosher [15], Kamotani and Greber [16] and others, provide measured values of the pressure distribution on the surface surrounding the jet

orifice which have been used to compare the accuracy of predictive models. During the past few years, a number of approximate methods to predict the pressure distribution has been developed: Wooler [17,18], Wu and Wright [19], Adler and Baron [20] and Schmitt [21]. Again, because of the complex nature of the flow, all these models have utilized some degree of empiricism. Either the model is formulated using experimentally obtained trajectory expressions or the model is formulated using analytical expressions whose coefficients are selected to provide best fit with experimental data. The majority of the models are based on integral techniques with simplifying assumptions, such as (i) the representation of the entire flow as two-dimensional [19], (ii) the external flow is irrotational, uncompressible and steady-state [20] or (iii) the flow is inviscid except that viscosity is the mechanism that leads to entrainment [18].

With the aid of these assumptions, the following approaches were made. Adler and Baron formulated their model by integrating momentum equations to describe the jet mixing field, without using empirical trajectory data. However, numerous parameters were derived using empirical correlations from prior research. Their results provide satisfactory agreement with experiment, but from the quantity of empiricism involved, one might expect such agreement. Wooler [17] followed by Wu and Wright [19] utilized blockage-sink representations where entrainment of crossflow fluid was handled analytically with suitably chosen coefficients. Again the results had satisfactory

agreement with experiment. However, an earlier effort by Wooler [18] minimized empiricism to the extent that only an experimentally determined jet trajectory was necessary to complete the model. By thus restricting the number of empirical parameters, this model has considerable appeal from an engineering point of view. Since visualization of actual jet-crossflow situations has shown that the jet is deflected in the crossflow direction and forms two contra-rotating trailing vortices, this interference model was based on the representation of the jet by a distribution of vorticity. Incorporating arguments from the aerodynamic theory of lifting bodies this vorticity distribution was quantitatively described along the experimentally determined trajectory. By virtue of minimal empiricism and therefore greater appeal, this model was selected as the basis for continued investigation in developing a better predictive tool.

III. REVIEW OF WOOLER'S VORTEX MODEL

Before any attempt to develop an improved model was made, a detailed re-derivation of the basis formulation was performed in order to: (1) gain a better understanding of the logic of formulation and (2) confirm the reported results. A review of the distributed vortex method follows.

One area of interest was the geometry of the problem. The empirical trajectory equation used was

$$x/d = B\left[\cosh(z/Bd) - 1\right] \tag{4}$$

where x is measured in the direction of the mainstream and z is measured in the direction of the exiting jet. The coefficient B was empirically determined from Jordinson [11] and is equal to $0.19\ (U_j/U)^2$, where U_j is the jet velocity and U is the mainstream velocity. To further describe the problem (see Fig. 2), a system of natural coordinates attached to the jet is adopted. Relative to the fixed coordinate system and an arbitrary point $\left[x_p, y_p\right]$ on the surface surrounding the jet orifice, the natural coordinates are given by

$$\begin{aligned} \xi &= -\left[z\sin\alpha + (x-x_p)\cos\alpha\right] \\ \eta &= Y_p \\ \zeta &= z\cos\alpha - (x-x_p)\sin\alpha \end{aligned} \tag{5}$$

where ξ is the coordinate tangent to the jet; ζ, the coordinate normal to the jet in the direction of the center of

curvature; η, the coordinate perpendicular to ξ and ζ ; and α , the angle between the x and ξ directions.

Another extremely important part of Wooler's formulation was the calculation of the distribution of vorticity within the jet. This distribution of vorticity was determined by adopting methods commonly found in the aerodynamic theory of lifting surfaces [22]. According to this theory, regions of flow external to the jet are taken to be irrotational and the deflection of the jet is due to a purely inviscid mechanism. This inviscid mechanism is expressed as a balance between the forces due to pressure differences across an element of the jet and the centrifugal forces associated with the jet curvature. These pressure differences define corresponding velocity differences according to Bernoulli's Theorem. These resulting velocity differences, in turn, are related to circulation according to Kelvin's definition of circulation. Therefore, with the above assumptions, the circulation is related to jet curvature, and this relationship is

$$\frac{\Gamma}{U} = \frac{\pi}{4} \frac{d}{R} \left(\frac{U_j}{U} \right)^2 \tag{6}$$

where Γ is the circulation per unit length, ds, along the jet; R, the local radius of curvature of the jet; and d, the diameter of the jet orifice. Utilizing the empirical trajectory expression [Eq. (4)] in the arc length derivative results in

$$\frac{ds}{R} = \frac{1}{Bd} \frac{dz}{\cosh(z/Bd)} \tag{7}$$

Incorporating Eq. (7) into Eq. (6) and integrating over an element of jet extending from z_1 to z_2 results in the following expression for the circulation of a jet element

$$K = \frac{\pi}{2} Ud \left(\frac{U_j}{U}\right)^2 \left[\tan^{-1} e^{z_2/Bd} - \tan^{-1} e^{z_1/Bd}\right] \quad (8)$$

In order to determine the flow field disturbance on the plate, the jet was divided into a number of vortex elements whose strengths were calculated using Eq. (8). These elements are the origins of characteristic horseshoe vortex systems where the cross member is bound in the jet and the trailing sides are, according to Wooler's assumption, tangent to the jet and separated by a distance, d, the diameter of the jet orifice (Fig. 3). Errors associated with taking the trailing vortices tangent to the jet instead of containing them within the jet as in the actual flow situation were assumed by Wooler to have negligible effect on the velocity field along the plate. Each of these horseshoe vortex systems produces an interference velocity on the surface surrounding the jet orifice. To determine this interference velocity at any arbitrary point on the surface, the Law of Biot and Savart [23]

$$\vec{q} = \frac{K}{4\pi} \int_L \frac{\vec{ds} \times \vec{r}}{r^3}$$

is applied to each bound vortex and its associated trailing vortices. For the bound vortex, $-d/2 \leq L \leq d/2$, and for the trailing vortices, $z_i \leq L \leq \infty$, were the integration limits. These integrations produced closed-form solutions for the interference velocities due to individual jet elements. The

total interference velocity components due to the entire jet are determined as the sum of elemental contributions and are given by

$$\frac{u}{U} = \frac{1}{8}\left(\frac{U_j}{U}\right)^2 \sum_{i=1}^{N} \left[\tan^{-1}\left(\frac{e^{z_{i+1}/Bd} - e^{z_i/Bd}}{1+e^{(z_{i+1} + z_i)/Bd}}\right)\right] \times \left[(-w_1+w_2-w_3)\sin\alpha_i + u_1\cos\alpha_i\right]$$

$$\frac{v}{U} = \frac{1}{8}\left(\frac{U_j}{U}\right)^2 \sum_{i=1}^{N} \left[(-v_2+v_3)\tan^{-1}\left(\frac{e^{z_{i+1}/Bd} - e^{z_i/Bd}}{1 + e^{(z_{i+1} + z_i)/Bd}}\right)\right]$$

where N is the number of jet elements and z_i and z_{i+1} are the endpoints of the general element. The parameters u, v and w are defined as geometric coefficients resulting from the integration along the jet. The subscripts 1, 2, 3 refer to the bound, left and right (as viewed from upstream) vortex contributions respectively. They are given by

$$u_1 = \frac{\zeta}{\xi^2+\zeta^2}\left[\frac{\eta + \frac{1}{2}}{\sqrt{\xi^2+\zeta^2+(\eta+\frac{1}{2})^2}} - \frac{\eta - \frac{1}{2}}{\sqrt{\xi^2+\zeta^2+(\eta-\frac{1}{2})^2}}\right]$$

$$v_2 = \frac{\zeta}{\zeta^2+(\eta-\frac{1}{2})^2}\left[1 + \frac{\xi}{\sqrt{\xi^2+\zeta^2+(\eta-\frac{1}{2})^2}}\right]$$

$$v_3 = \frac{\zeta}{\zeta^2+(\eta+\frac{1}{2})^2} + \left[1 \frac{\xi}{\sqrt{\xi^2+\zeta^2+(\eta+\frac{1}{2})^2}}\right]$$

$$w_1 = \frac{\xi}{\xi^2 + \zeta^2}\left[\frac{\eta + \frac{1}{2}}{\sqrt{\xi^2 + \zeta^2 + (\eta + \frac{1}{2})^2}} - \frac{\eta - \frac{1}{2}}{\sqrt{\xi^2 + \zeta^2 + (\eta - \frac{1}{2})^2}}\right]$$

$$w_2 = \frac{\eta - \frac{1}{2}}{\zeta^2 + (\eta - \frac{1}{2})^2}\left[1 + \frac{\xi}{\sqrt{\xi^2 + \zeta^2 + (\eta - \frac{1}{2})^2}}\right]$$

$$w_3 = \frac{\eta + \frac{1}{2}}{\zeta^2 + (\eta + \frac{1}{2})^2}\left[1 + \frac{\xi}{\sqrt{\xi^2 + \zeta^2 + (\eta + \frac{1}{2})^2}}\right]$$

and ξ, ζ , and η are given by Eq. (5) for each point on the surface. After calculation of the interference velocity vector at a sufficient number of points on the surface, the pressure coefficinet at each point, C_p, is given by

$$C_p = \frac{P - P_\infty}{\frac{1}{2}\rho U^2} = 1 - q^2/U^2$$

where $q^2/U^2 = \left(\frac{U + 2u}{U}\right)^2 + \left(\frac{2v}{U}\right)^2$. The double u and v components are the result of the use of an image system to establish the surface as a solid boundary thereby negating the w component of velocity in this plane. Upon substitution and simplification, one has

$$C_p = -4\left[\frac{u}{U} + \left(\frac{u}{U}\right)^2 + \left(\frac{v}{U}\right)^2\right] \qquad (9)$$

After completion of the review and the incorporation of several necessary corrections to the published work [18], the entire formulation was coded for computer solution. The resulting plots of pressure contours for representative

velocity ratios (Figs. 4,5,6) show fair agreement with the experiments of Bradbury and Wood [6]. However, these plots also point out serious deficiencies in the model. In the far field, in the arc $35^{\circ} < \theta < 145^{\circ}$ (θ being measured counter clockwise from the ray extending downstream from the jet origin), the method represents the jet interference effects well, but in both the upstream and downstream portions of the surface, there is a definite lack of agreement. In the upstream area, the blockage effect due to the presence of the jet in the uniform flow is not predicted, while in the downstream regions, additional wake effects have not been taken into account. However, in view of the large area of good agreement with experiment, Wooler's distributed vorticity model was selected as the foundation for further investigation. It is apparent that this model gives a fair representation of the actual contra-rotating vortices associated with the jet-crossflow interaction.

IV. EXTENSION OF WOOLER MODEL

Upon successful confirmation and correction of Wooler's distributed vortex model and as a step towards developing an improved model, it was felt necessary to verify the trailing vortex assumption, that these vortices are tangential to the jet rather than contained in the jet. Retaining the basic theoretical concepts for calculating the incremental circulation of a finite length of the jet, containment of the trailing vortices was approximated by successive conforming discretized vortex elements. These vortex elements were formed by restricting the length of the trailing vortices to the linear distance between z_1 and z_2, the arbitrarily-chosen end points of the finite length of jet, ds. In order to satisfy the Helmholtz vortex theorem, that a vortex cannot end in the fluid, the above horseshoe vortex system was closed by connecting the trailing arms with another bound, contra-rotating vortex. (See Fig. 7) By making this alteration, vortex loops of increasing incremental strength, as given by Eq. (8), can be made to conform to the curvature of the jet, as in the actual flow situation. This resulting vortex pattern is analogous to that created by a continuously accelerating wing [23]. As a wing accelerates, the strength of the produced vortices correspondingly increase, a situation very similar to the change in elemental vortex strength associated with the jet curvature.

Using this contained-vortex system, the interference velocity due to the jet at any arbitrary point on the plate was determined by applying the Biot-Savart Law (See Appendix A). In this application, it was necessary to approximate the trailing vortices as straight-line segments. However, as the sizes of the jet elements become small, the linear approximation can be made to conform to the curvature with an exactness that is only limited by numerical practicalities. The total interference components due to the entire jet result from the summation of elemental contributions and are given by

$$\frac{u}{U} = \frac{1}{8}\left(\frac{U_j}{U}\right)^2 \sum_{i=1}^{N} \left\{ \left[-w_1 \sin\alpha_i + w_2 \sin\alpha_{i+1} + (-w_3 + w_4)\sin\alpha_B + u_1 \cos\alpha_i - u_2 \cos\alpha_{i+1} \right] \times \sum_{k=1}^{i} \tan^{-1}\left(\frac{e^{z_{k+1}} - e^{z_k}}{1 + e^{(z_{k+1} + z_k)}} \right) \right\}$$

$$\frac{v}{U} = \frac{1}{8}\left(\frac{U_j}{U}\right)^2 \sum_{i=1}^{N} \left\{ \left[v_3 - v_4 \right] \times \sum_{k=1}^{i} \tan^{-1}\left(\frac{e^{z_{k+1}} - e^{z_k}}{1 + e^{(z_{k+1} + z_k)}} \right) \right\}$$

where N is the number of jet elements and z_k and z_{k+1} are the endpoints of the general element. Again, the parameters u, v, and w are defined as geometric coefficients resulting from applying the Biot-Savart Law around the element. The subscripts 1,2,3 and 4 refer to the forward and after bound and left and right trailing vortex contributions, respectively. These are given by

$$u_1 = \frac{\zeta_1}{\xi_1^2 + \zeta_1^2}\left[\frac{\eta + \frac{1}{2}}{\sqrt{\xi_1^2 + \zeta_1^2 + (\eta + \frac{1}{2})^2}} - \frac{\eta - \frac{1}{2}}{\sqrt{\xi_1^2 + \zeta_1^2 + (\eta - \frac{1}{2})^2}}\right]$$

$$u_2 = \frac{\zeta_2}{\xi_2^2 + \zeta_2^2}\left[\frac{\eta + \frac{1}{2}}{\sqrt{\xi_2^2 + \zeta_2^2 + (\eta + \frac{1}{2})^2}} - \frac{\eta - \frac{1}{2}}{\sqrt{\xi_2^2 + \zeta_2^2 + (\eta - \frac{1}{2})^2}}\right]$$

$$v_3 = \frac{\zeta_B}{\zeta_B^2 + (\eta - \frac{1}{2})^2}\left[\frac{\xi_{B2}}{\sqrt{\xi_{B2}^2 + \zeta_B^2 + (\eta - \frac{1}{2})^2}} - \frac{\xi_{B1}}{\sqrt{\xi_{B1}^2 + \zeta_B^2 + (\eta - \frac{1}{2})^2}}\right]$$

$$v_4 = \frac{\zeta_B}{\zeta_B^2 + (\eta + \frac{1}{2})^2}\left[\frac{\xi_{B2}}{\sqrt{\xi_{B2}^2 + \zeta_B^2 + (\eta + \frac{1}{2})^2}} - \frac{\xi_{B1}}{\sqrt{\xi_{B1}^2 + \zeta_B^2 + (\eta + \frac{1}{2})^2}}\right]$$

$$w_1 = \frac{\xi_1}{\xi_1^2 + \zeta_1^2}\left[\frac{\eta + \frac{1}{2}}{\sqrt{\xi_1^2 + \zeta_1^2 + (\eta + \frac{1}{2})^2}} - \frac{\eta - \frac{1}{2}}{\sqrt{\xi_1^2 + \zeta_1^2 + (\eta - \frac{1}{2})^2}}\right]$$

$$w_2 = \frac{\xi_2}{\xi_1^2 + \zeta_2^2}\left[\frac{\eta + \frac{1}{2}}{\sqrt{\xi_2^2 + \zeta_2^2 + (\eta + \frac{1}{2})^2}} - \frac{\eta - \frac{1}{2}}{\sqrt{\xi_2^2 + \zeta_2^2 + (\eta - \frac{1}{2})^2}}\right]$$

$$w_3 = \frac{\eta - \frac{1}{2}}{\zeta_B^2 + (\eta - \frac{1}{2})^2}\left[\frac{\xi_{B2}}{\sqrt{\xi_{B2}^2 + \zeta_B^2 + (\eta - \frac{1}{2})^2}} - \frac{\xi_{B1}}{\sqrt{\xi_{B1}^2 + \zeta_B^2 + (\eta - \frac{1}{2})^2}}\right]$$

$$w_4 = \frac{\eta + \frac{1}{2}}{\zeta_B^2 + (\eta + \frac{1}{2})^2}\left[\frac{\xi_{B2}}{\sqrt{\xi_{B2}^2 + \zeta_B^2 + (\eta + \frac{1}{2})^2}} - \frac{\xi_{B1}}{\sqrt{\xi_{B1}^2 + \zeta_B^2 - (\eta + \frac{1}{2})^2}}\right]$$

where the various ξ's, ζ's and η's are given by Equations (A1, A2, A3) of Appendix A. With these interference velocity components at numerous points on the plate, the pressure coefficient, Eq. (9), was determined for selected points

on the plate. The resulting contours of constant pressure coefficient are shown in Figs. 8, 9, and 10.

These resulting plots show a somewhat different agreement with the experimental data [6] than did the results of Wooler's model; however, the discrepancy can be directly attributed to the manner in which the trailing vortices are treated. In Wooler's model, the total interference velocity due to the trailing vortices results from the cumulative elemental vortices acting at different distances relative to a point on the surface, while in the conforming vortex model the trailing vortex contribution results from the cumulative elemental vortex strength acting at a single radius, (See Fig. 11). Therefore, Wooler's assumption of treating the trailing vortices as being tangent to the trajectory introduced an error that under some conditions tended to improve agreement, where the conforming vortex model removed this error at the expense of some loss in agreement, at least at the larger values of U_j/U. However, there have been studies [12,21] that present the concept of an effective origin of the jet vortex system - a region where the turbulent mixing processes extend across the entire jet causing definite deflection of the jet and establishment of the contrarotating vortices. Schmidt [21] formulated an empirical expression for the position of the effective source as a function of the jet-to-mainstream velocity ratio given by

$$Z_e = (15\ \sigma\sqrt{\sigma})^{-1}$$

where $\sigma = U/U_j$. Applying this effective source expression

to the conforming vortex model produces better agreement with experiment (Fig. 12).

Comparison of the conforming vortex model, including an effective source, with experimental data shows the same, if not better, far-field agreement with an improvement in the predicted pressure distribution in upstream and downstream regions. Therefore, this model which more closely represents the actual flow situation, replaced Wooler's model as the basis for further investigation and improvement.

V. IMPROVEMENT OF CONFORMING VORTEX MODEL

Evaluation of the conforming vortex model results indicated the continued lack of agreement with experiment in two distinct areas: upstream and wake. In order to improve the agreement in these areas, it was felt that additional corrections could be formulated from a qualitative analysis of the flow phenomenon. The discrepancies in the upstream area can be, at least partially, attributed to the blockage of the mainstream flow by the presence of the jet, while the discrepancies in the wake area are caused by turbulent flow separation, vortex shedding and turbulent entrainment. In view of the present uncertainty concerning the exact character of the wake area, it was decided that the development of corrections for the wake must await future investigation and experimentation. Therefore, the upstream blockage correction was undertaken.

Near the point of injection, the physical appearance of a circular jet injected into a crossing flow is that of a cylinder. Interpreting the jet as a cylinder in an irrotational flow, potential flow theory predicts perturbations to the uniform flow that are given by

$$\frac{u}{U} = -\frac{a^2}{r^2} \cos 2\theta$$

$$\frac{v}{U} = -\frac{a^2}{r^2} \sin 2\theta \qquad (10)$$

where r and θ are cylindrical coordinates of points in the flow field and a is the radius of the cylinder. These velocity perturbations caused by blockage can be combined with the interference velocity components derived from the vorticity formulation to adjust the coefficient of pressure (Eq. 9) at arbitrary points on the surface. The initial (and most simple) assumption was to make the diameter of the blockage cylinder the same as the diameter of the jet orifice. The resulting pressure distribution indicated an excessive blockage that is not present in the real flow. The actual flow does not produce a solid interface, as would a cylinder, but instead an entraining interface surrounding a core of uniform velocity approximately equal to U_j, the jet exit velocity. To better describe this, a potential cylinder of diameter less than the diameter of the jet was introduced. Using many combinations of cylinder diameters with different jet-to-mainstream velocity ratios, an expression for a in Eq. (10) was formulated in terms of the velocity ratio.

$$a = 0.96 \sqrt{\sigma}$$

Applying this formulation to the blockage-cylinder perturbation velocity calculations results in pressure contour plots (Fig. 13,14,15) that show improved agreement with experiment in the far field and upstream areas for jet-to-mainstream velocity ratios, $4 \leq \frac{1}{\sigma} \leq 8$. However, as the velocity ratio increases, the model results and experiment diverge. The apparent cause of this disagreement can be resolved by qualitatively examining the actual flow. With increasing

velocity ratios, the entrainment of crossflow fluid by the jet becomes the more dominant interference factor, while the blockage factor is relatively less important. Wu and Wright [19] have concluded that "the amount of crosswind fluid entrained increases with increasing jet speed" when the crosswind speed is held constant. In addition, this increased entrainment appears to be especially important in the downsteam wake region and causes a further reduction in the blockage effect as compared to that due to a solid cylinder in a crossflow. The resulting effect of the increased rate of entrainment at higher jet speeds is larger interference velocity perturbations in the flow field surrounding the jet orifice near the plate. In view of this, the lack of agreement at higher velocity ratios can be explained while also pointing out the need for additional correction(s) to account for the change in the relative importance of blockage and entrainment with changes in velocity ratio.

VI. CURRENT MODEL CAPABILITY

Realizing the limitations of the current analytical model, it is nevertheless appropriate to investigate its predictive capability. Figure 16 shows the results of the analysis expressed as the force induced on a flat plate due to a jet injected at right angles to a crossflow. The force is expressed as a fraction of the ideal jet thrust and the negative values indicate suction forces (in a direction opposite to the ideal jet thrust). Correlation with experiment [4] shows a difference in the value of k in Eq. (2). The value of $k \approx -4.4$ resulting from this analysis, although not in the predicted range, $-3.0 \leq k \leq -1.5$, still displays the correct trend and provides encouragement as to the potential success of a model based upon the present methods. The main difference in the approximation constant results from the lack of proper accounting for the entire entrainment effect, a factor which progressively degrades the model at higher velocity ratios. However, as an initial design approximation for low velocity bow thrusters active at relatively high ship speeds, the conforming vortex model presented here provides a satisfactory prediction of the interference effects -- a step toward improving the accuracy of powering and control determinations.

VII. CONCLUSIONS

The conforming vortex model, modified with corrections based on experimental observations, is presented as an initial formulation of a simple yet physically consistent representation of jet-crossflow interference effects. Pressure distributions in the far-field are adequately predicted and the calculated results obtained with the model provide reasonably good agreement with experiment for the lower jet-to-crossflow velocity ratios. Agreement is less than satisfactory for the higher velocity ratios. However, the model does indicate the relative importance of different flow phenomena with changing velocity ratios. The most evident weakness of the model is the lack of an adequate method for including entrainment and blockage effects near to the origin of the jet at higher velocity ratios. By restricting the range of application, the conforming vortex model demonstrates sufficient agreement to be utilized as a first approximation technique for designing bow thrusters.

VIII. RECOMMENDATIONS

Further experiments should be conducted to provide more correlation data, especially in the case of water jet into water crossflow. Empirical constants utilized in the current model and those that will become necessary when trying to model increased entrainment can be refined when a larger data base is available. The encouraging results of this method of analyzing the flow field should not be overlooked, and additional corrections, as indicated in this analysis, should be made to improve its accuracy.

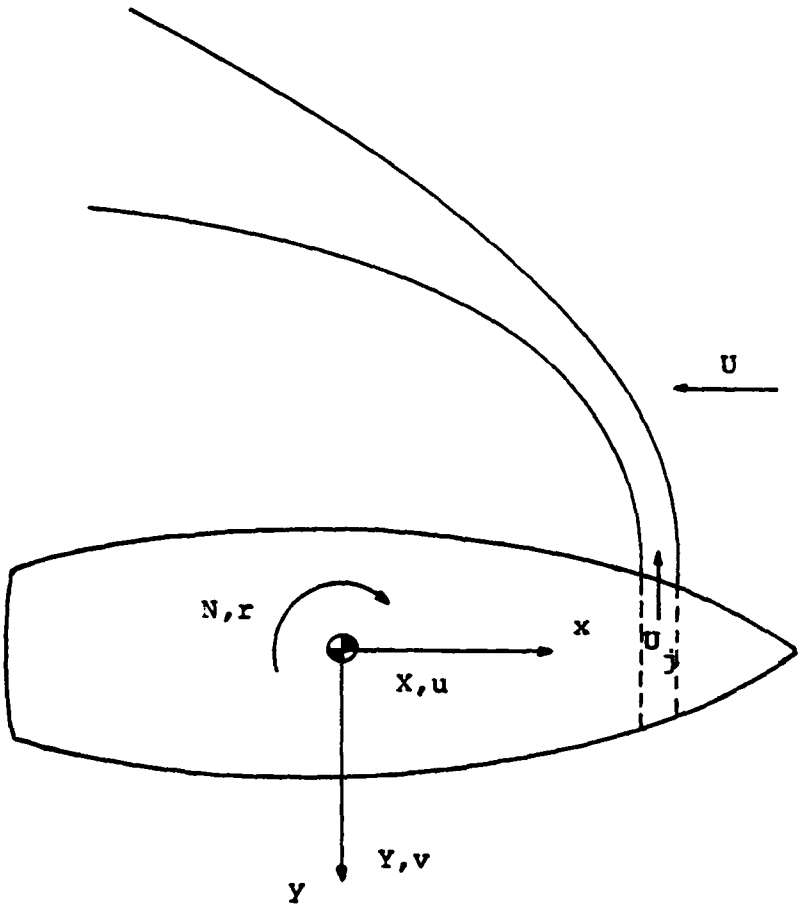

Figure 1. Sketch of bow thruster-crossflow interaction.

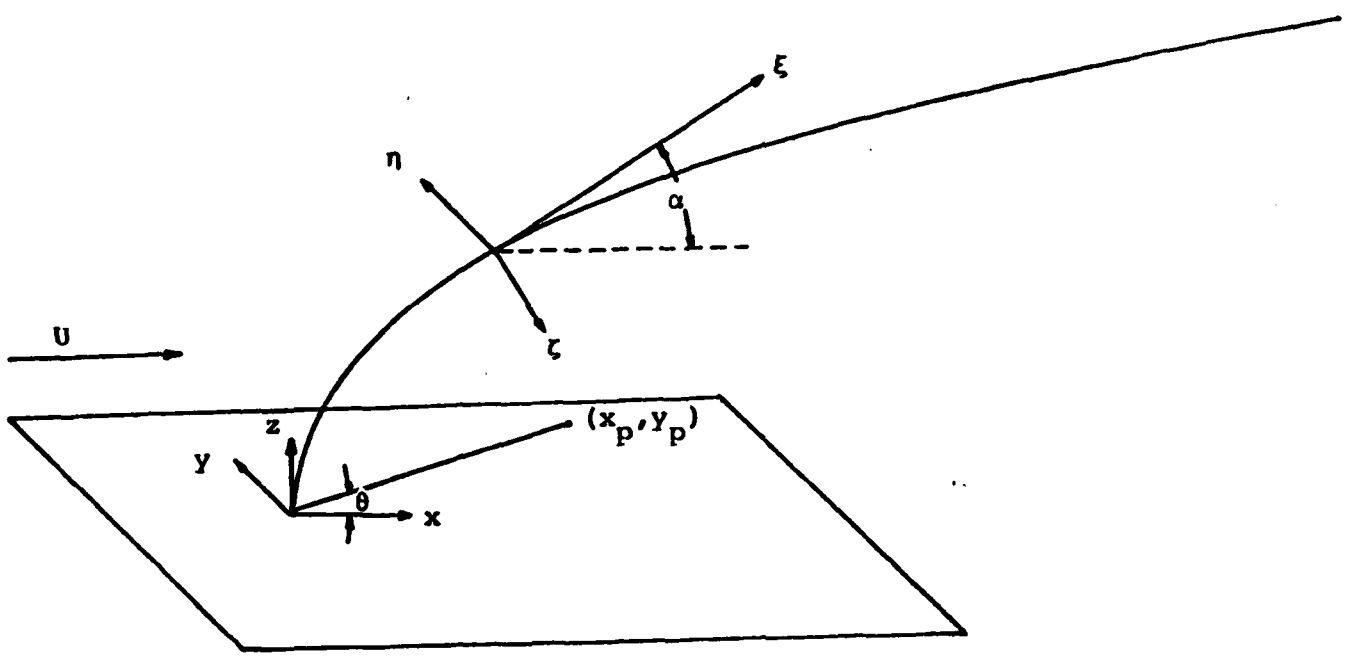

Figure 2. Description of coordinate systems.

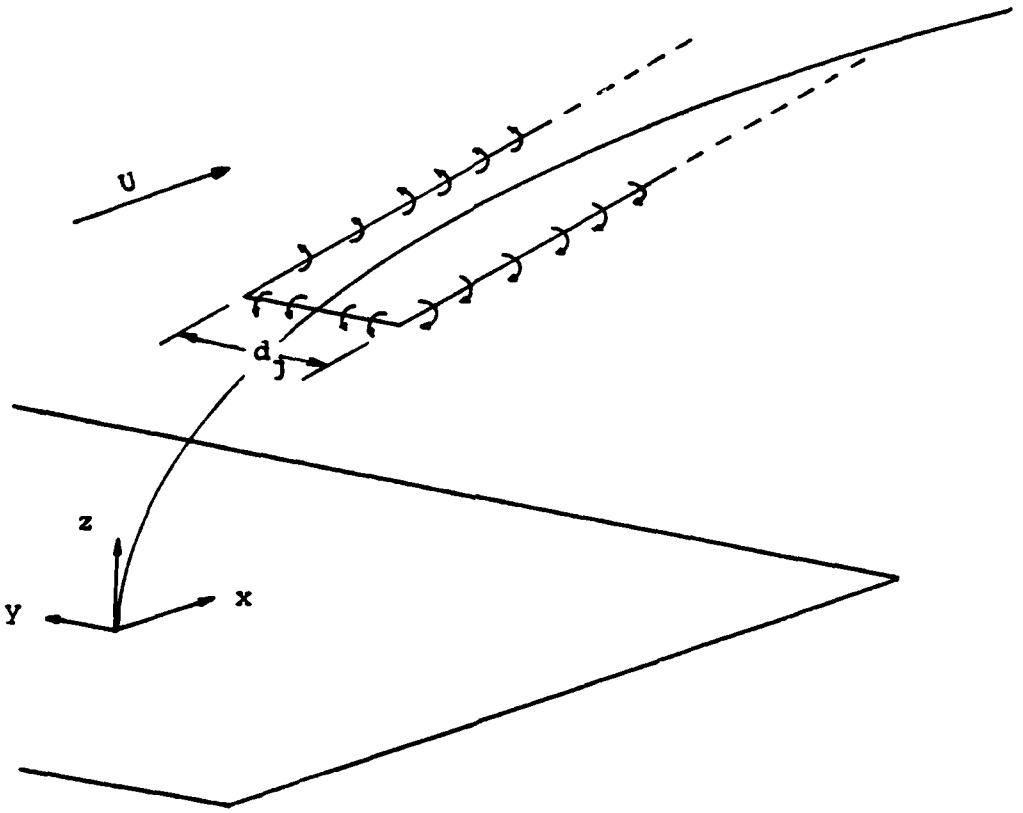

Figure 3. Wooler Horseshoe Vortex System

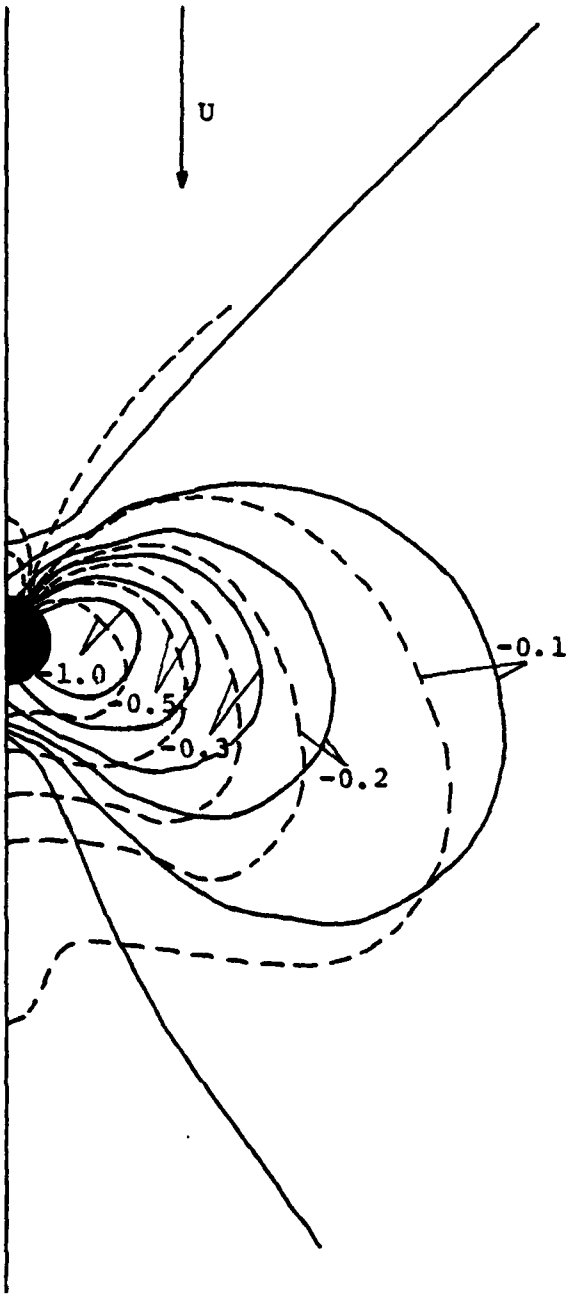

Figure 4. Comparison Of Pressure Coefficient Contours
Experiment ---[6], Wooler ———
Velocity Ratio = 4

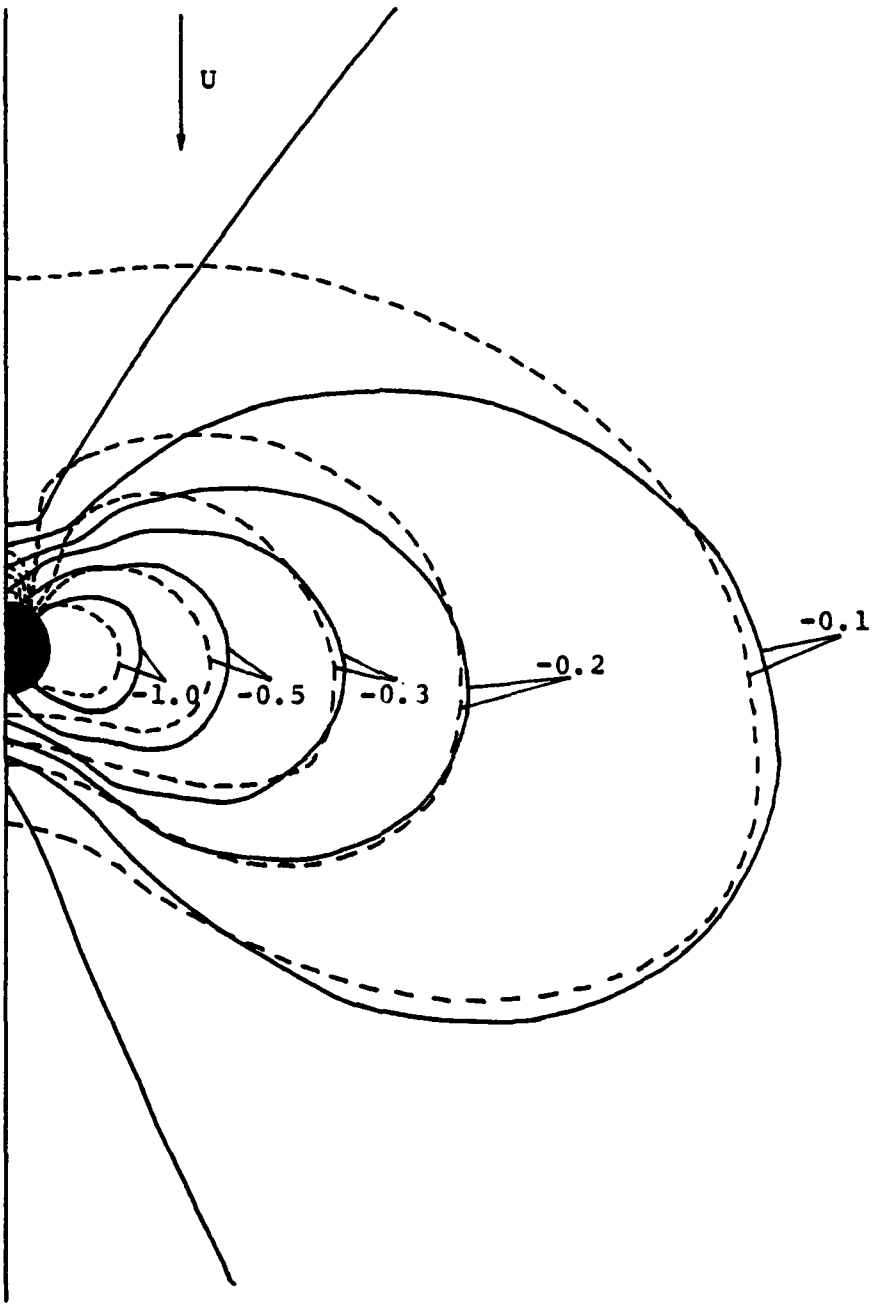

Figure 5. Comparison Of Pressure Coefficient Contours
Experiment ---[6], Wooler ———
$U_j/U = 8$

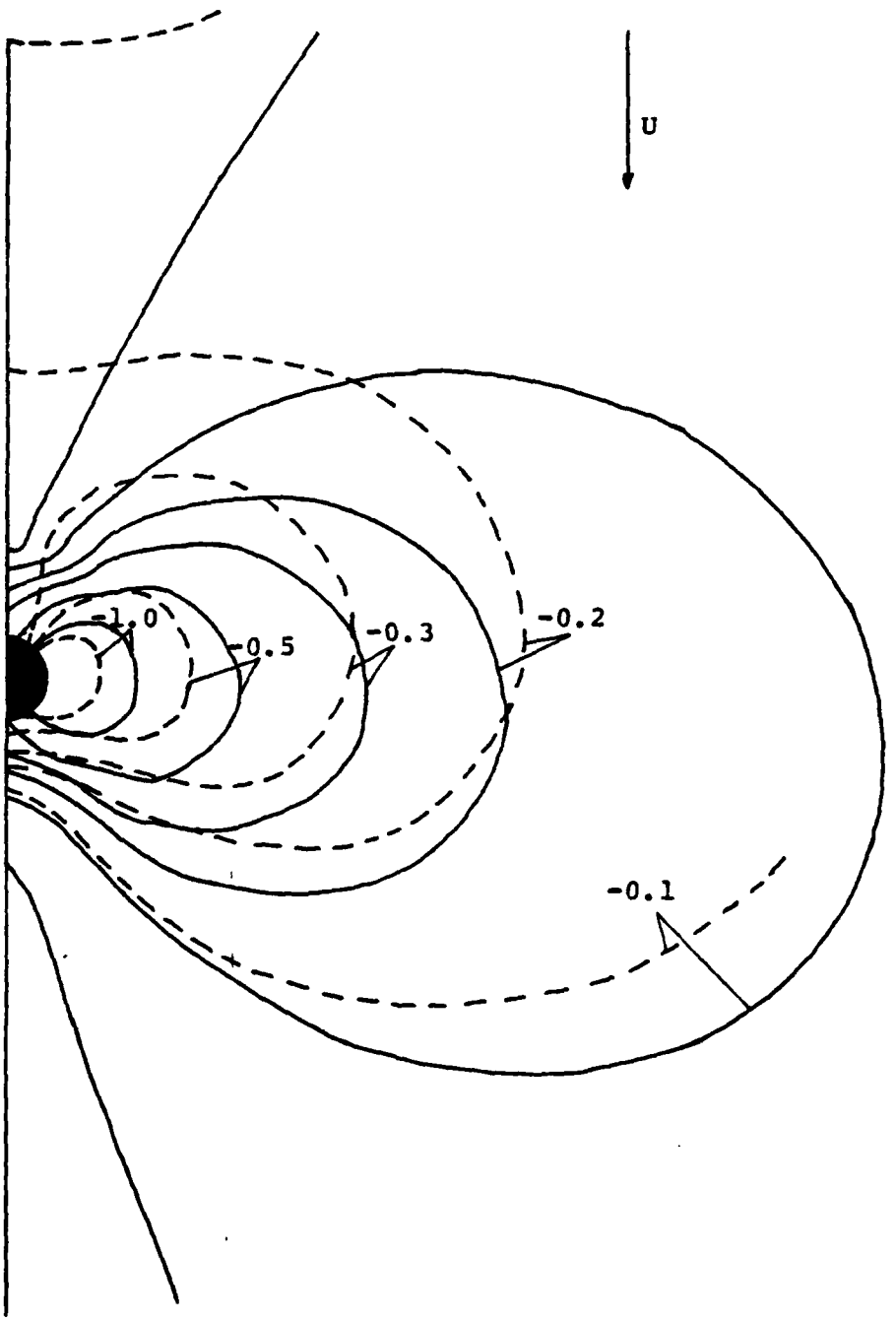

Figure 6. Comparison Of Pressure Coefficient Contours
Experiment ---[6], Wooler ———
$U_j/U = 11.3$

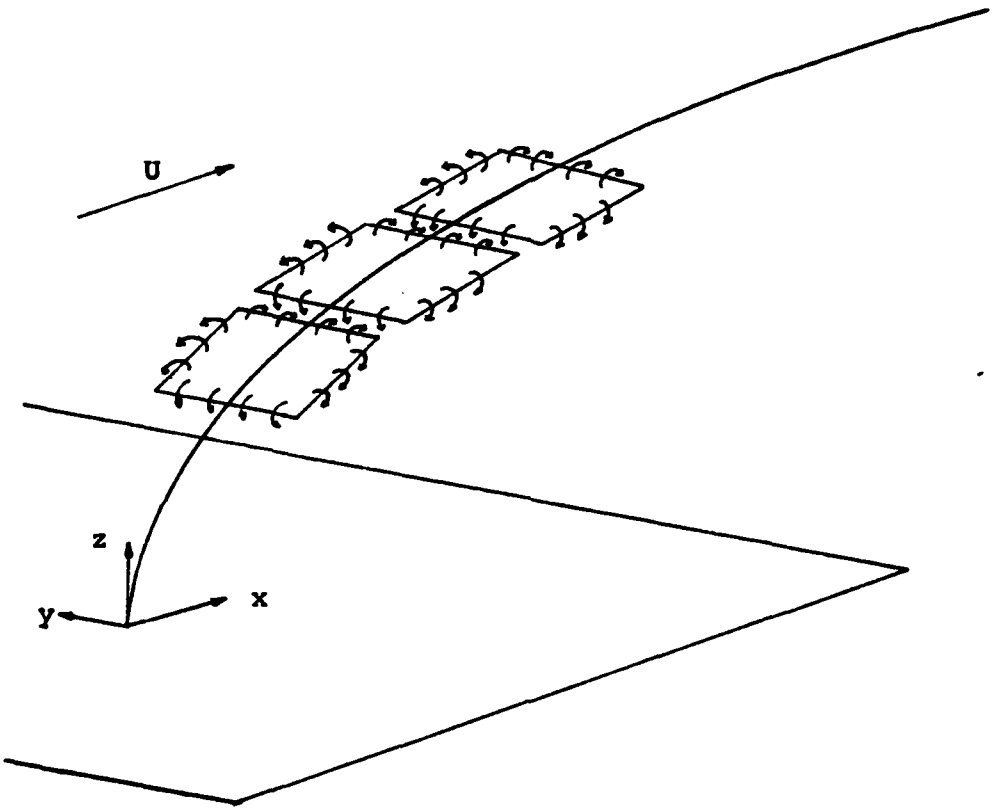

Figure 7. Conforming Vortex Loop System

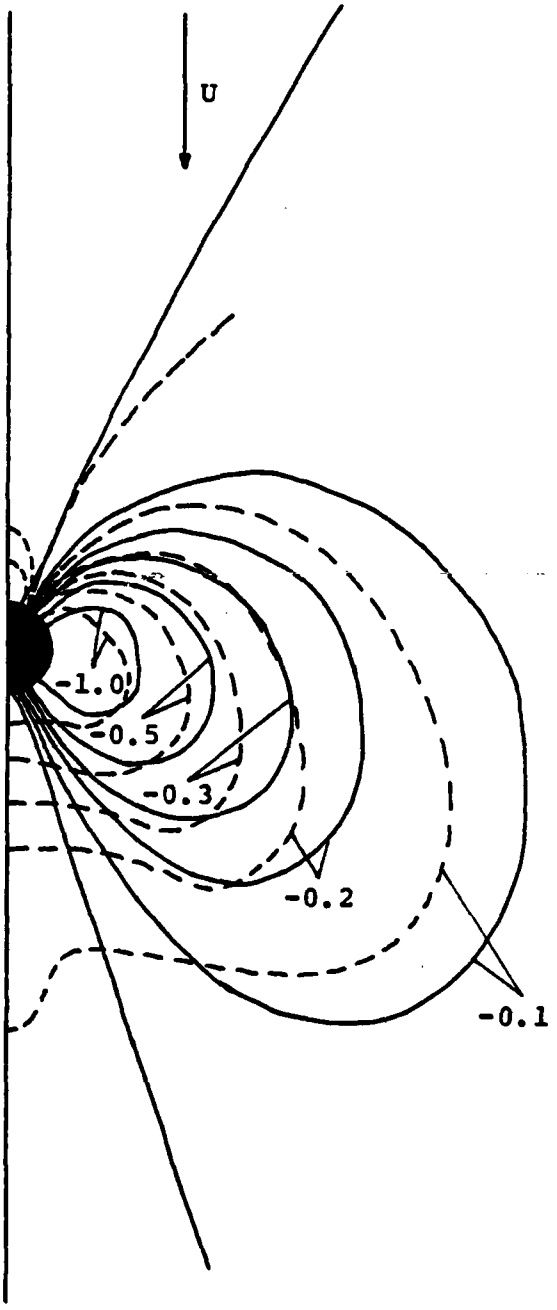

Figure 8. Comparison Of Pressure Coefficient Contours Experiment ---[6], Conforming Vortex Model ——— $U_j/U = 4.0$.

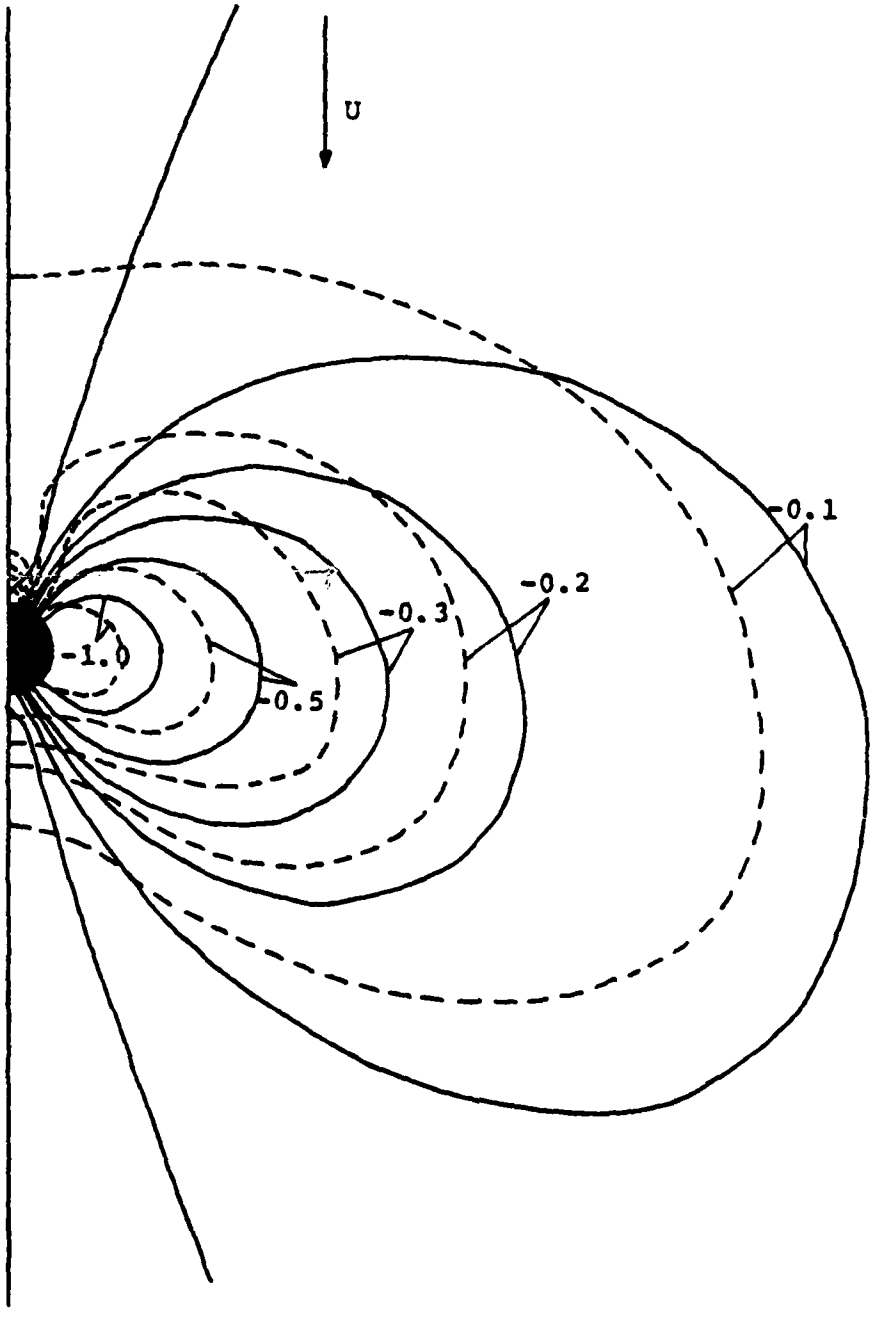

Figure 9. Comparison Of Pressure Coefficient Contours Experiment ---[6], Conforming Vortex Model ——— $U_j/U = 8.0$

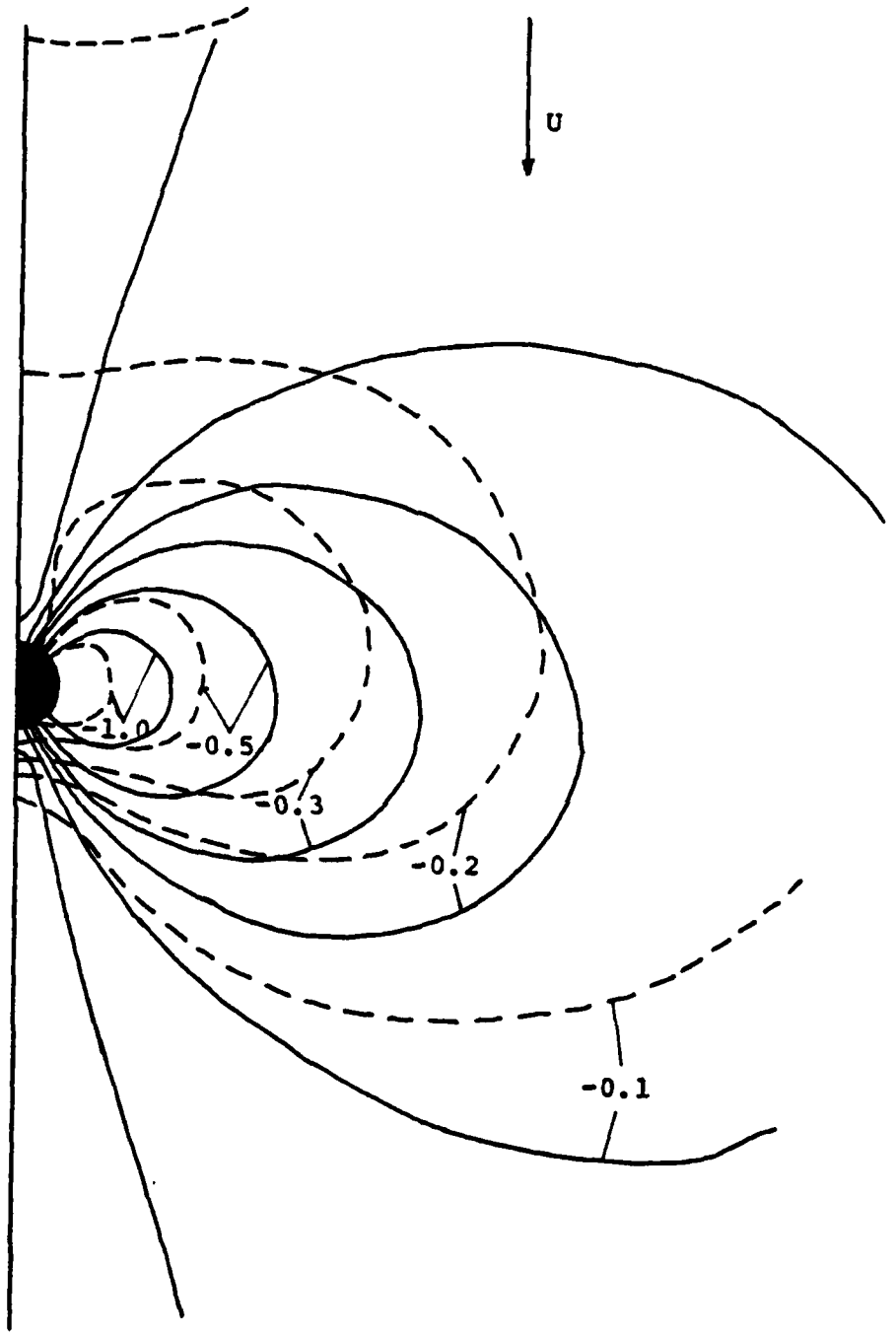

Figure 10. Comparison Of Pressure Coefficient Contours Experiment ---[6], Conforming Vortex Model ——— $U_j/U = 11.3$

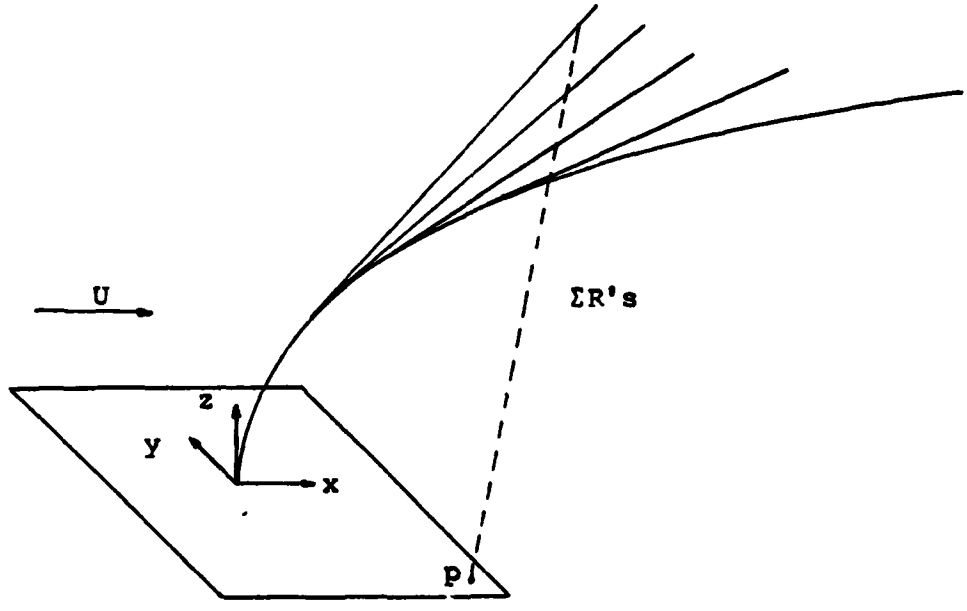

Figure a. Wooler Model

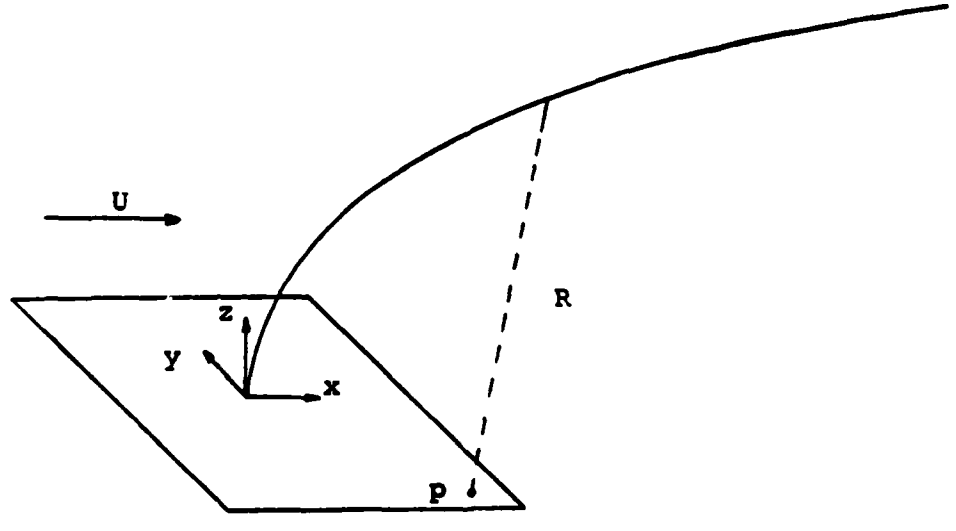

Figure b. Conforming Vortex Model

Figure 11. Comparison Of Wooler (a) And Conforming Vortex Model (b) Effective Radii For Induced Velocities

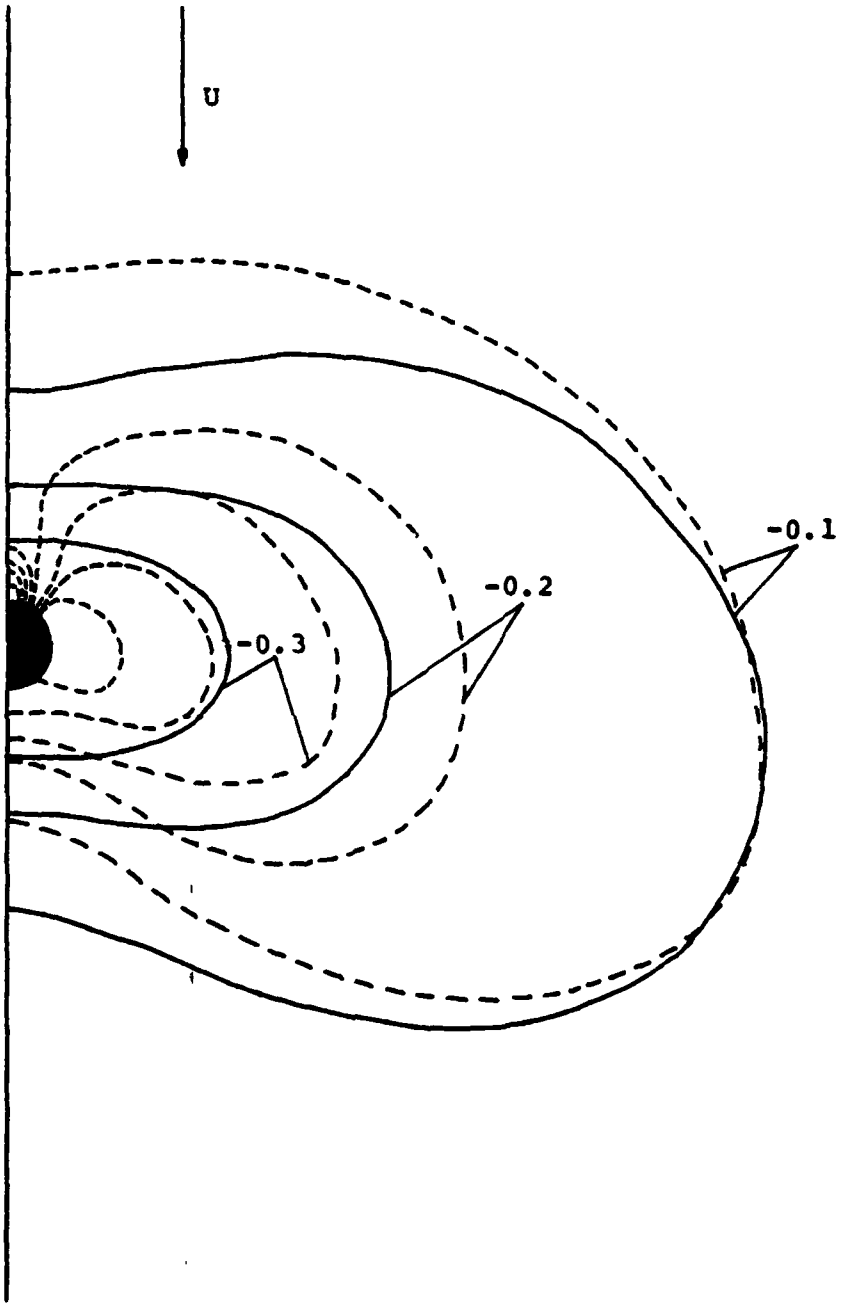

Figure 12. Comparison Of Pressure Coefficient Contours Experiment ---[6], Conforming Vortex Model With Effective Source Correction——. $U_j/U = 8.0$

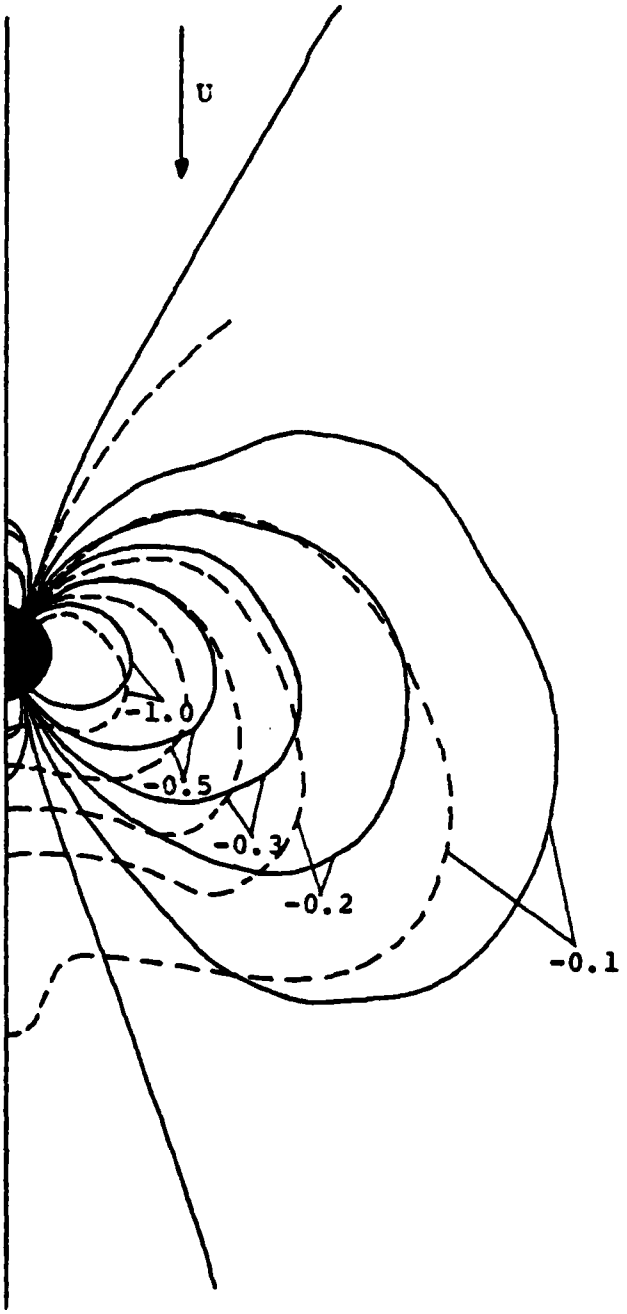

Figure 13. Comparison Of Pressure Coefficient Contours Experiment ---[6], Fully Corrected Conforming Vortex Model—. $U_j/U = 4.0$

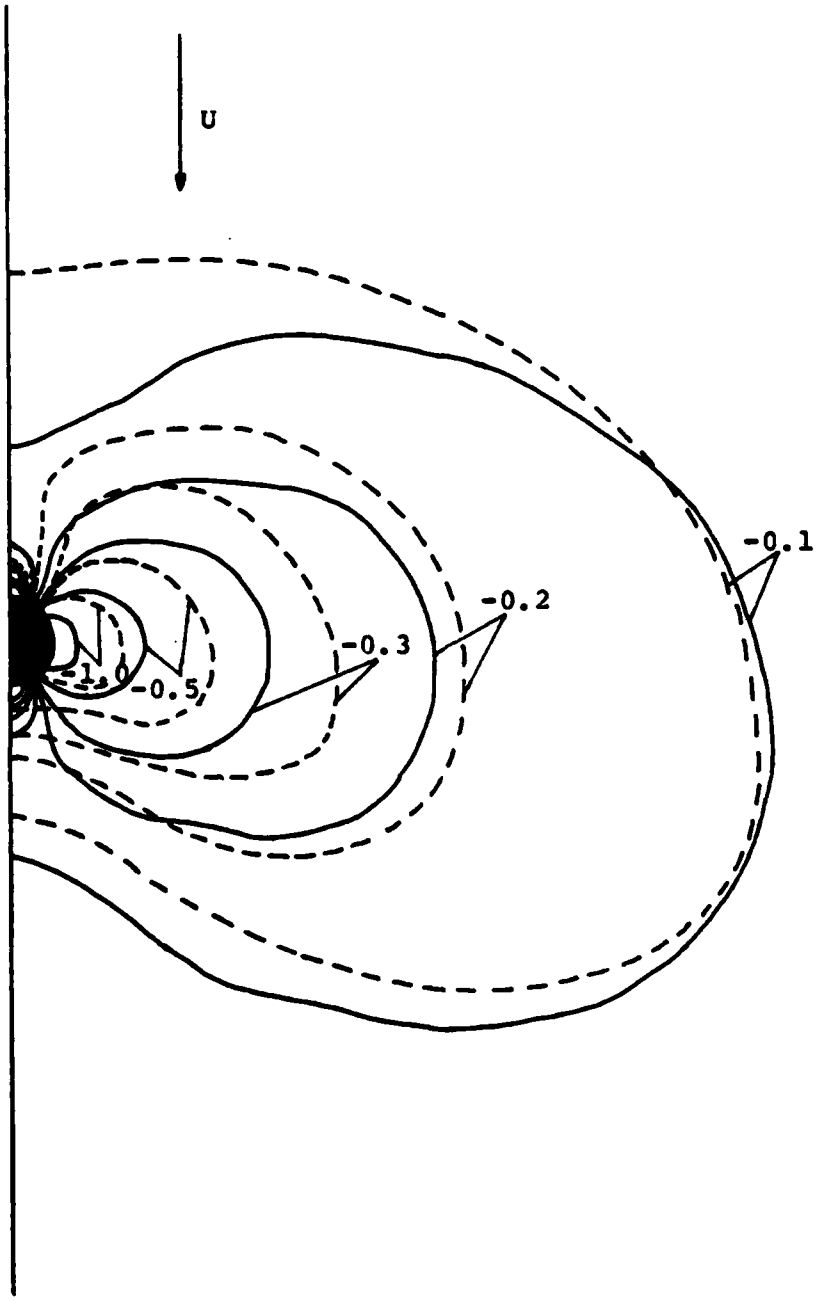

Figure 14. Comparison Of Pressure Coefficient Contours Experiment ---[6,7], Fully Corrected Conforming Vortex Model—, $U_j/U = 8.0$

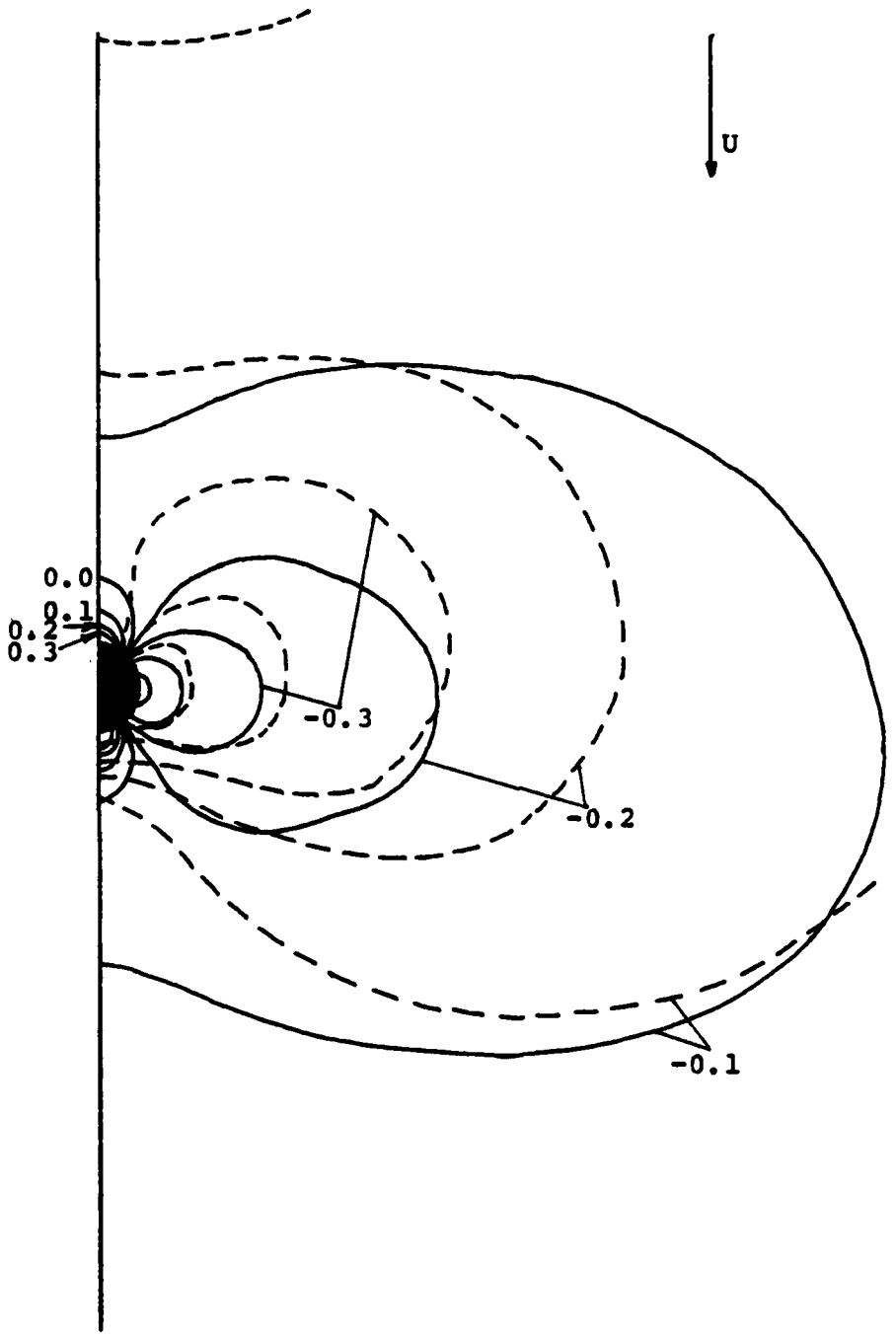

Figure 15. Comparison Of Pressure Coefficient Contours Experiment ---[6], Fully Corrected Conforming Vortex Model——. U_j/U = 11.3

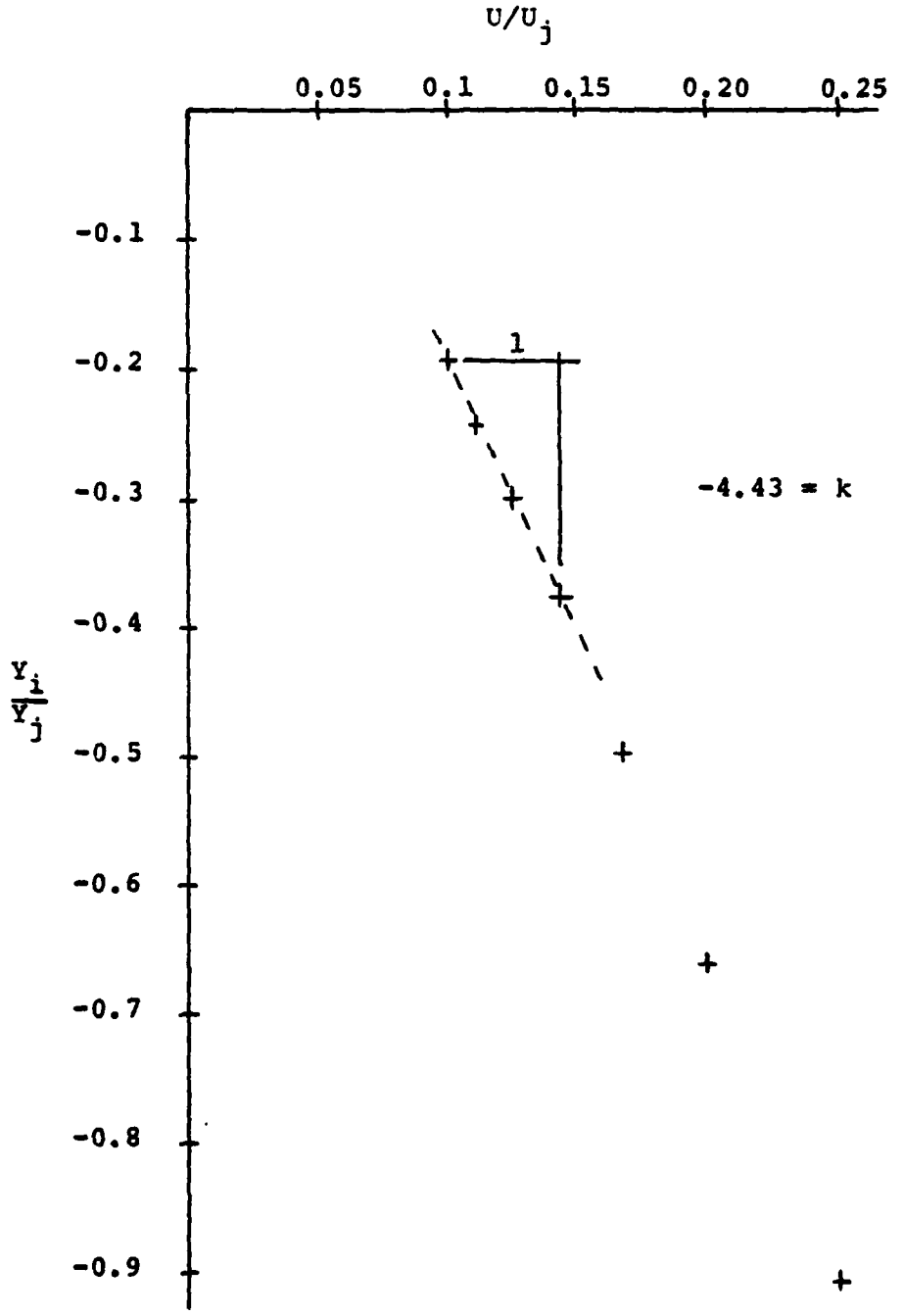

Figure 16. Variation In The Induced Force Due To Jet-Crossflow Interaction

APPENDIX A

FORMULATION OF INTERFERENCE VELOCITY COMPONENTS

The formulation of the interference velocity due to the vortex loop system of the conforming vortex model is given below. The formulation requires the use of three separate coordinate systems that are functions of the endpoints of a jet element and the position of an arbitrary point on the plate. From Fig. (A1), these are given by:

$$\xi_1 = -\left[z_1 \sin\alpha_1 + (x_1 - x_p)\cos\alpha_1\right] \tag{A1}$$

$$\eta = y_p$$

$$\zeta_1 = z_1\cos\alpha_1 - (x_1 - x_p)\sin\alpha_1$$

for the upstream bound vortex

$$\xi_2 = -\left[z_2 \sin\alpha_2 + (x_2 - x_p)\cos\alpha_2\right] \tag{A2}$$

$$\eta = y_p$$

$$\zeta_2 = z_2\cos\alpha_2 - (x_2 - x_p)\sin\alpha_2$$

for the downstream bound vortex, and

$$\xi_{Bi} = -\left[z_i \sin\alpha_B + (x_i - x_p)\cos\alpha_B\right]$$

$$\eta = y_p \tag{A3}$$

$$\zeta_B = z_i\cos\alpha_B - (x_i - x_p)\sin\alpha_B$$

for the trailing vortices, where x_p and y_p are the coordinates of an arbitrary point on the plate and x_1, z_1 x_2, z_2 are the coordinates of the endpoints of an element of jet. The angles α_1, α_2 and α_B are the angles between the x-direction and respective ξ's and are given by

$$\alpha_1 = \tan^{-1}\left[\operatorname{csch}\,(z_1/B)\right]$$

$$\alpha_1 = \tan^{-1}\left[\operatorname{csch}\,(z_2/B)\right]$$

$$\alpha_B = \tan^{-1}\left[(z_2 - z_1)/(x_2 - x_1)\right]$$

To determine the induced velocity at an arbitrary point, the law of Biot and Savart

$$|q| = \frac{\Gamma}{4\pi}\int_L \frac{\sin\beta}{r^2}\,ds \qquad \text{(A4)}$$

must be individually applied to both the bound and trailing vorticies. Due to similarities in the integrations, only one bound and one trailing vortex formulation will be presented and necessary changes applied for the other vortices. The circulation of a finite amount of jet, given by [Eq. (8)]

$$K = \frac{\pi}{2}\,Ud\left(\frac{U_j}{U}\right)^2\left[\tan^{-1} e^{z_2/Bd} - \tan^{-1} e^{z_1/Bd}\right]$$

is the incremental contribution which is added to each successive element, such that the total circulation for a given element is given by

$$\Gamma_n = \frac{\pi}{2} Ud \left(\frac{U_j}{U}\right)^2 \sum_{k=1}^{n} \left[\tan^{-1} e^{z_{k+1}/Bd} - \tan^{-1} e^{z_k/Bd}\right] \tag{A5}$$

Therefore, the induced velocity due to any of the vortex filaments associated with the n-th element, $1 \leq n \leq N$, where N is the number of jet elements, can be determined from

$$|q_n| = \frac{\Gamma_n}{4\pi} \int_L \frac{\sin\beta}{r^2} \, ds \tag{A6}$$

where L is the length of the filament, β is the angle between the vortex filament and the radius, r, to an arbitrary point on the plate.

For the forward bound vortex (See Fig. (A2))

$$\sin\beta = \frac{\sqrt{\xi_1^2 + \zeta_1^2}}{\sqrt{\xi_1^2 + \zeta_1^2 + (\eta + s)^2}}$$

and

$$r^2 = \xi_1^2 + \zeta_1^2 + (\eta + s)^2$$

Substituting these equations into Eq. (A6) gives

$$|q_{n1}| = \frac{\Gamma_n}{4\pi} \int_L \frac{\sqrt{\xi_1^2 + \zeta_1^2}}{\left[\xi_1^2 + \zeta_1^2 + (\eta + s)^2\right]^{3/2}} \, ds \tag{A7}$$

the magnitude of the induced velocity at an arbitrary point on the plate due to the bound vortex of the n-th element. The x-direction component of this velocity is given by

$$q_{x1} = |q_{n1}| \left[\cos\gamma_1 \cos\alpha_1 - \sin\gamma_1 \sin\alpha_1\right] \tag{A8}$$

where $\cos\gamma_1 = \dfrac{\zeta_1}{\sqrt{\xi_1^2 + \zeta_1^2}}$ and $\sin\gamma_1 = \dfrac{\xi_1}{\sqrt{\xi_1^2 + \zeta_1^2}}$.

Inserting Eq. (A7) into Eq. (A8) and applying the integration limits gives

$$q_{x1} = \frac{\Gamma_n}{4\pi}\left[\int_{-\frac{1}{2}}^{\frac{1}{2}} \frac{\zeta_1}{\left[\xi_1^2 + \zeta_1^2 + (\eta + s)^2\right]^{3/2}}\, ds \cos\alpha_1 - \right. \tag{A9}$$

$$\left. \int_{-\frac{1}{2}}^{\frac{1}{2}} \frac{\xi_1}{\left[\xi_1^2 + \zeta_1^2 + (\eta + s)^2\right]^{3/2}}\, ds \sin\alpha_1 \right]$$

Integration of Eq. (A9) results in

$$q_{x1} = \frac{\Gamma_n}{4\pi}\left[\frac{\zeta_1}{\xi_1^2 + \zeta_1^2}\left(\frac{\eta + \frac{1}{2}}{\sqrt{\xi_1^2 + \zeta_1^2 + (\eta + \frac{1}{2})^2}} - \frac{\eta - \frac{1}{2}}{\sqrt{\xi_1^2 + \zeta_1^2 + (\eta - \frac{1}{2})^2}}\right)\cos\alpha_1\right.$$

$$\left. - \frac{\xi_1}{\xi_1^2 + \zeta_1^2}\left(\frac{\eta + \frac{1}{2}}{\sqrt{\xi_1^2 + \zeta_1^2 + (\eta + \frac{1}{2})^2}} - \frac{\eta + \frac{1}{2}}{\sqrt{\xi_1^2 + \zeta_1^2 + (\eta - \frac{1}{2})^2}}\sin\alpha_1\right)\right] \tag{A10}$$

the x-direction component of induced velocity due to the forward bound vortex. Similarly, the x-direction component of induced velocity due to the downstream bound vortex is given by

$$q_{x2} = \frac{\Gamma_n}{4\pi}\left[- \frac{\zeta_2}{\xi_2^2 + \zeta_2^2}\left(\frac{\eta + \frac{1}{2}}{\sqrt{\xi_2^2 + \zeta_2^2 + (\eta + \frac{1}{2})^2}} - \frac{\eta - \frac{1}{2}}{\sqrt{\xi_2^2+\zeta_2^2+(\eta-\frac{1}{2})^2}}\right)\cos\alpha_2 \right.$$

$$\left. - \frac{\xi_2}{\xi_2^2 + \zeta_2^2}\left(\frac{\eta + \frac{1}{2}}{\sqrt{\xi_2^2+\zeta_2^2+(\eta+\frac{1}{2})^2}} - \frac{\eta - \frac{1}{2}}{\sqrt{\xi_2^2+\zeta_2^2+(\eta-\frac{1}{2})^2}}\right)\sin\alpha_2\right] \tag{A11}$$

The approximation of the bound vortices as being linear eliminates the y-direction component of induced velocity and since an image system is utilized to formulate the flat plate, it is unnecessary to calculate any z-direction component of induced velocity.

For the left trailing vortex filament, as viewed from upstream (See Fig. (A3)).

$$\sin\beta = \frac{\sqrt{\zeta_B^2 + (\eta - \frac{1}{2})^2}}{\sqrt{\zeta_B^2 + (\eta - \frac{1}{2})^2 + s^2}}$$

$$r^2 = \zeta_B^2 + (\eta - \tfrac{1}{2})^2 + s^2$$

Inserting these expressions into Eq. (A6) gives

$$\left|q_{n3}\right| = \frac{\Gamma_n}{4\pi}\int_L \frac{\sqrt{\zeta_B^2 + (\eta - \frac{1}{2})^2}}{\left[\zeta_B^2 + (\eta - \frac{1}{2})^2 + s^2\right]^{3/2}} ds \tag{A12}$$

the magnitude of the induced velocity at an arbitrary point on the plate due to the left trailing vortex of the n-th element. Resolving this velocity into x and y components gives

$$q_{x3} = - \left|q_{n3}\right| \cos\gamma_B \sin\alpha_B$$

and (A13)

$$q_{y3} = \left|q_{n3}\right| \sin\gamma_B$$

where $\cos\gamma_B = \dfrac{\eta - \frac{1}{2}}{\sqrt{\zeta_B^2 + (\eta - \frac{1}{2})^2}}$ and $\sin\gamma_B = \dfrac{\zeta_B}{\sqrt{\zeta_B^2 + (\eta - \frac{1}{2})^2}}$

Inserting Eq. (A12) into Eq. (A13) and applying integration limits gives

$$q_{x3} = - \frac{\Gamma_n}{4\pi} \int_{\xi_{B1}}^{\xi_{B2}} \frac{\eta - \frac{1}{2}}{\left[\zeta_B^2 + (\eta - \frac{1}{2})^2 + s^2\right]^{3/2}} ds \sin\alpha_B$$

$$q_{y3} = \frac{\Gamma_n}{4\pi} \int_{\xi_{B1}}^{\xi_{B2}} \frac{\zeta_B}{\left[\zeta_B^2 + (\eta - \frac{1}{2})^2 + s^2\right]^{3/2}} ds \qquad \text{(A14)}$$

Integration of Eq. (A14) yields

$$q_{x3} = - \frac{\Gamma_n}{4\pi} \left[\frac{\eta - \frac{1}{2}}{\zeta_B^2 + (\eta - \frac{1}{2})^2} \left(\frac{\xi_{B2}}{\sqrt{\zeta_B^2 + (\eta - \frac{1}{2})^2 + \xi_{B2}^2}} - \frac{\xi_{B1}}{\sqrt{\zeta_B^2 + (\eta - \frac{1}{2})^2 + \xi_{B1}^2}} \right) \sin\alpha_B \right]$$

$$q_{y3} = \frac{\Gamma_n}{4\pi} \left[\frac{\zeta_B}{\zeta_B^2 + (\eta - \frac{1}{2})^2} \left(\frac{\xi_{B2}}{\sqrt{\zeta_B^2 + (\eta - \frac{1}{2})^2 + \xi_{B2}^2}} - \frac{\xi_{B1}}{\sqrt{\zeta_B^2 + (\eta - \frac{1}{2})^2 + \xi_{B1}^2}} \right) \right]$$

(A15)

the x and y components of induced velocity due to the left trailing vortex. Similarly the x and y components of the induced velocity due to the right trailing vortex are given by

$$q_{x4} = \frac{\Gamma_n}{4\pi}\left[\frac{\eta + \frac{1}{2}}{\zeta_B^2 + (\eta + \frac{1}{2})^2}\left(\frac{\xi_{B2}}{\sqrt{\zeta_B^2+(\eta+\frac{1}{2})^2+\xi_{B2}^2}} - \frac{\xi_{B1}}{\sqrt{\zeta_B^2+(\eta+\frac{1}{2})^2+\xi_{B1}^2}}\right)\sin\alpha_B\right.$$

$$q_{y4} = -\frac{\Gamma_n}{4\pi}\left[\frac{\zeta_B}{\zeta_B^2 + (\eta + \frac{1}{2})^2}\left(\frac{\xi_{B2}}{\sqrt{\zeta_B^2+(\eta+\frac{1}{2})^2+\xi_{B2}^2}} - \frac{\xi_{B1}}{\sqrt{\zeta_B^2+(\eta+\frac{1}{2})^2+\xi_{B1}^2}}\right)\right] \tag{A16}$$

Therefore, the total x and y components of induced velocity due to an entire element of jet are

$$q_{xT} = q_{x1} + q_{x2} + q_{x3} + q_{x4}$$
$$q_{yT} = q_{y3} + q_{y4} \tag{A17}$$

Inserting Eqs.(A10), (A11), (A15), and (A16) into Eq. (A14) yields

$$q_{xT} = \frac{\Gamma_n}{4\pi}\left[u_1\cos\alpha_1 - u_2\cos\alpha_2 - w_1\sin\alpha_1 + w_2\sin\alpha_2 + (-w_3+w_4)\sin\alpha_B\right]$$
$$q_{yT} = \frac{\Gamma_n}{4\pi}\left[v_3 - v_4\right] \tag{A18}$$

where

$$u_1 = \frac{\zeta_1}{\xi_1^2 + \zeta_1^2}\left[\frac{\eta + \frac{1}{2}}{\sqrt{\xi_1^2+\zeta_1^2+(\eta+\frac{1}{2})^2}} - \frac{\eta - \frac{1}{2}}{\sqrt{\xi_1^2+\zeta_1^2+(\eta-\frac{1}{2})^2}}\right]$$

$$u_2 = \frac{\zeta_2}{\xi_2^2 + \zeta_2^2}\left[\frac{\eta + \frac{1}{2}}{\sqrt{\xi_2^2+\zeta_2^2+(\eta+\frac{1}{2})^2}} - \frac{\eta - \frac{1}{2}}{\sqrt{\xi_2^2+\zeta_2^2+(\eta-\frac{1}{2})^2}}\right]$$

$$v_3 = \frac{\zeta_B}{\zeta_B^2 + (\eta-\frac{1}{2})^2}\left[\frac{\xi_{B2}}{\sqrt{\xi_{B2}^2+\zeta_B^2+(\eta-\frac{1}{2})^2}} - \frac{\xi_{B1}}{\sqrt{\xi_{B1}^2+\zeta_B^2+(\eta-\frac{1}{2})^2}}\right]$$

$$v_4 = \frac{\zeta_B}{\zeta_B^2 + (\eta+\frac{1}{2})^2}\left[\frac{\xi_{B2}}{\sqrt{\xi_{B2}^2+\zeta_B^2+(\eta+\frac{1}{2})^2}} - \frac{\xi_{B1}}{\sqrt{\xi_{B1}^2+\zeta_B^2+(\eta+\frac{1}{2})^2}}\right]$$

$$w_1 = \frac{\xi_1}{\xi_1^2 + \zeta_1^2}\left[\frac{\eta + \frac{1}{2}}{\sqrt{\xi_1^2+\zeta_1^2+(\eta+\frac{1}{2})^2}} - \frac{\eta - \frac{1}{2}}{\sqrt{\xi_1^2+\zeta_1^2+(\eta-\frac{1}{2})^2}}\right]$$

$$w_2 = \frac{\xi_2}{\xi_2^2 + \zeta_2^2}\left[\frac{\eta + \frac{1}{2}}{\sqrt{\xi_2^2+\zeta_2^2+(\eta+\frac{1}{2})^2}} - \frac{\eta - \frac{1}{2}}{\sqrt{\xi_2^2+\zeta_2^2+(\eta-\frac{1}{2})^2}}\right]$$

$$w_3 = \frac{\eta - \frac{1}{2}}{\zeta_B^2 + (\eta-\frac{1}{2})^2}\left[\frac{\xi_{B2}}{\sqrt{\xi_{B2}^2+\zeta_B^2+(\eta-\frac{1}{2})^2}} - \frac{\xi_{B1}}{\sqrt{\xi_{B1}^2+\zeta_B^2+(\eta-\frac{1}{2})^2}}\right]$$

$$w_4 = \frac{\eta + \frac{1}{2}}{\zeta_B^2 + (\eta+\frac{1}{2})^2}\left[\frac{\xi_{B2}}{\sqrt{\xi_{B2}^2+\zeta_B^2+(\eta+\frac{1}{2})^2}} - \frac{\xi_{B1}}{\sqrt{\xi_{B1}^2+\zeta_B^2+(\eta+\frac{1}{2})^2}}\right]$$

Substituting the expression for Γ_n from Eq.(A5) into Eqs. (A18) and non-dimensionalizing yields

$$\frac{u}{U} = \frac{1}{8}\left(\frac{U_j}{U}\right)^2 \sum_{i=1}^{N}\left\{\left[-w_1\sin\alpha_i + w_2\sin\alpha_{i+1} + (-w_3+w_4)\sin\alpha_B + u_1\cos\alpha_i - u_2\cos\alpha_{i+1}\right] \times \sum_{k=1}^{i} \tan^{-1}\left(\frac{e^{z_{k+1}} - e^{z_k}}{1 + e^{(z_{k+1}+z_k)}}\right)\right\}$$

$$\frac{v}{U} = \frac{1}{8}\left(\frac{U_j}{U}\right)^2 \sum_{i=1}^{N}\left\{\left[v_3 - v_4\right] \times \sum_{k=1}^{i} \tan^{-1}\left(\frac{e^{z_{k+1}} - e^{z_k}}{1 + e^{(z_{k+1}+z_k)}}\right)\right\}$$

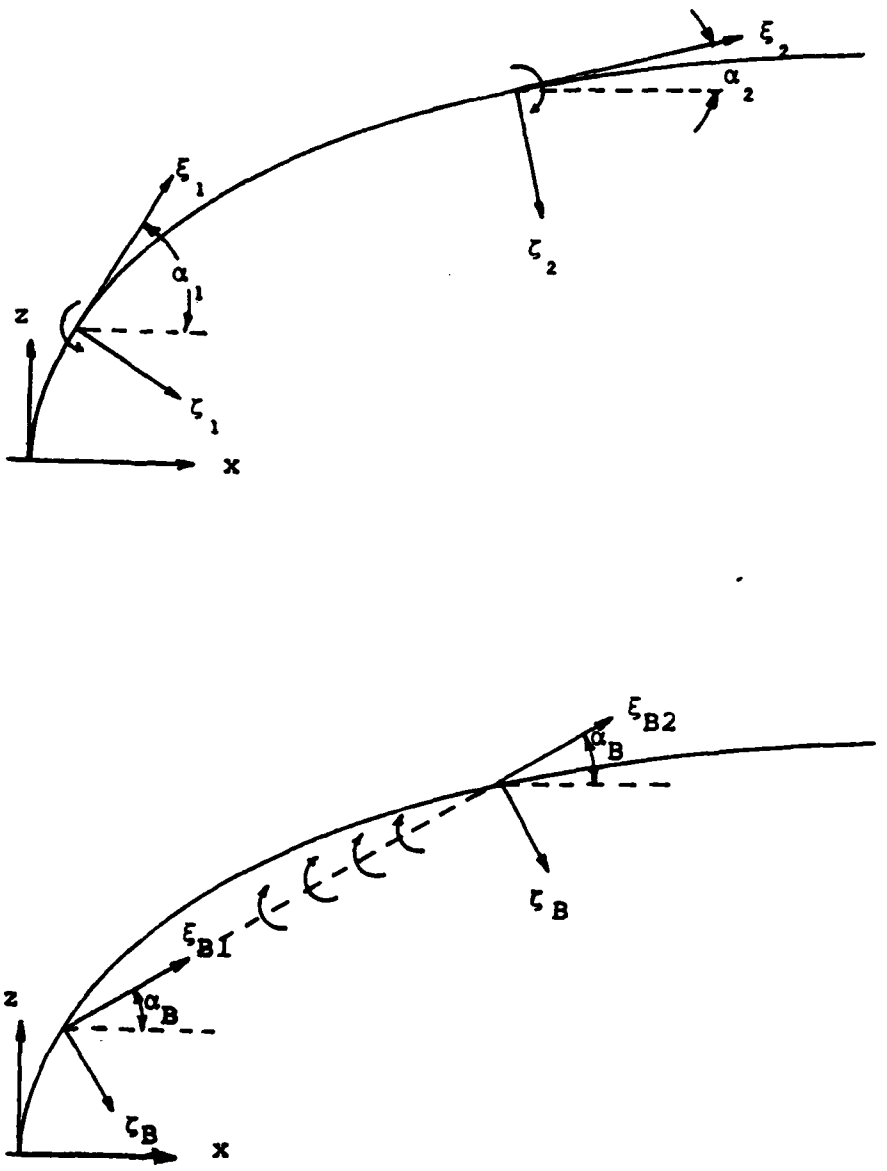

Figure A1. Coordinate Systems For Conforming Vortex Model

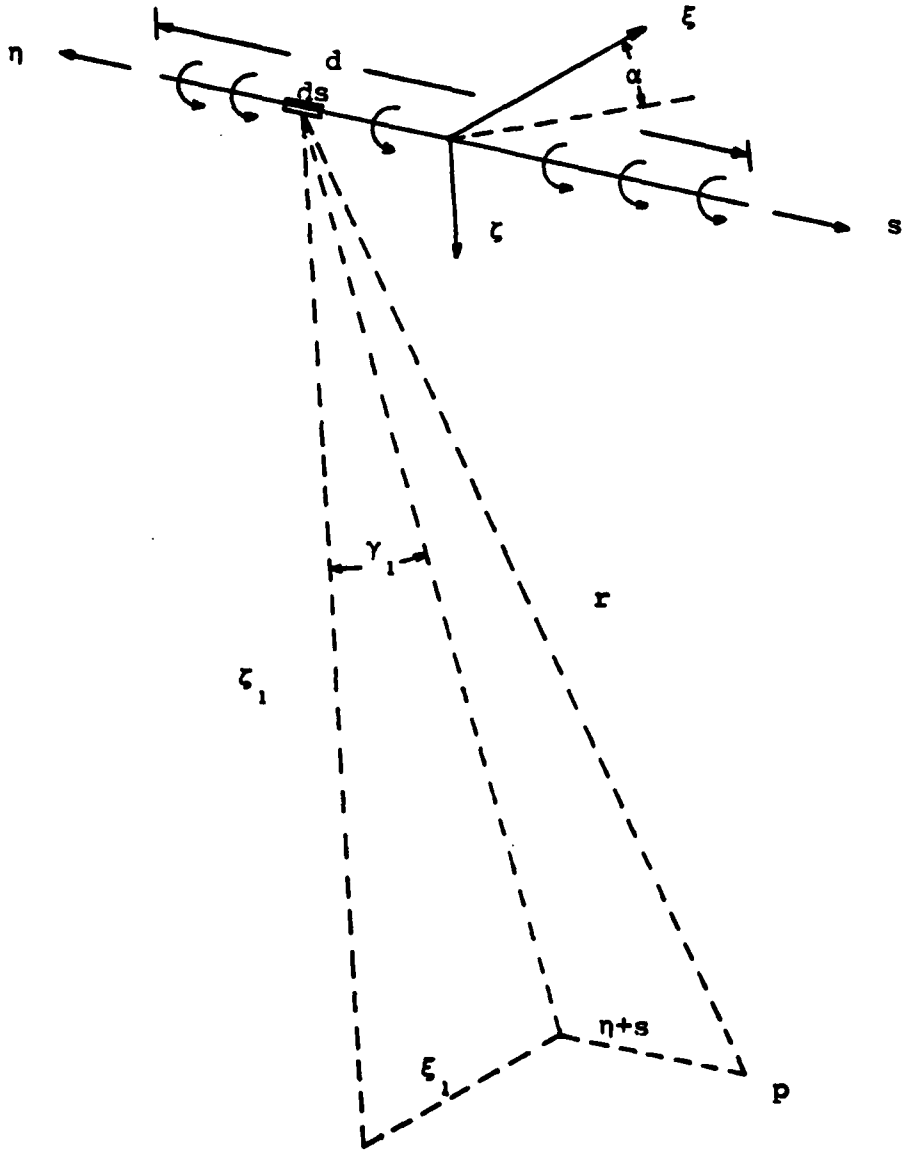

Figure A2. Geometry Of Bound Vortex Integration

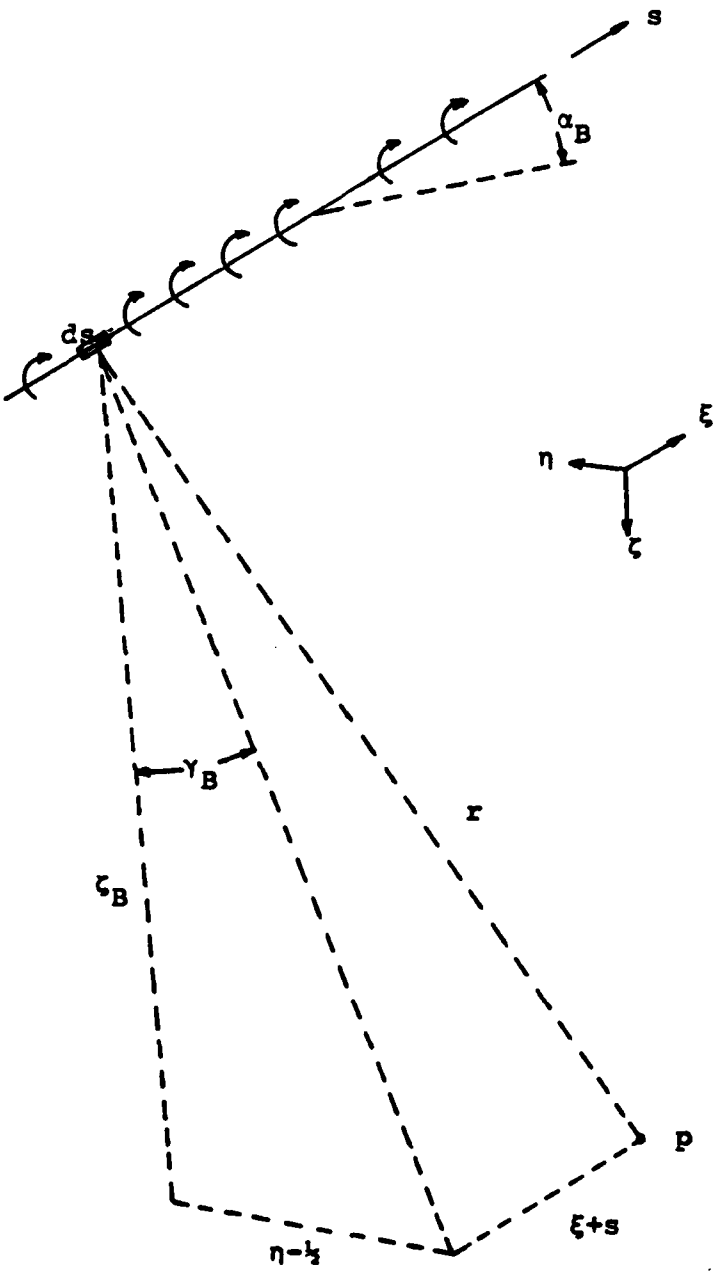

Figure A3. Geometry Of Trailing Vortex Integration

```
C                    XXXXXXXXXXXXXXXXXXXXXXXXXX
C                    X                        X
C                    X THIS PROGRAM SIMULATES A X
C                    X FLUID JET INJECTED INTO  X
C                    X A UNIFORM CROSSFLOW AND  X
C                    X FURTHER DETERMINES THE   X
C                    X PRESSURE DISTRIBUTION ON X
C                    X THE SURFACE FROM WHICH   X
C                    X THE JET IS EJECTED       X
C                    X                        X
C                    XXXXXXXXXXXXXXXXXXXXXXXXXX
C
C   DEFINITION OF TERMS
C
C     NTYPE  - MODEL TYPE:C-CONFORM
C                         1-CONFORM BLOCKAGE
C                         2-RAISED CONFORM
C                         3-RAISED CONFORM BLOCKAGE
C                              (INPUT)
C
C     NRAD   - NUMBER OF RADIAL POSITIONS ON SURFACE
C                (INPUT)
C
C     NANG   - NUMBER OF ANGULAR POSITIONS ON SURFACE
C                (INPUT)
C
C     NPOINT - NUMBER OF ARBITRARY POINTS ON SURFACE
C                (NRAD*NANG)
C
C     UJ     - JET VELOCITY (INPUT)
C
C     UM     - MAIN STREAM VELOCITY (INPUT)
C
C     D      - ACTUAL DIAMETER OF JET ORIFICE (INPUT)
C
C     R      - NON-DIMENSIONAL RADIAL POSITION OF SURFACE
C                POINTS (DIMENSIONED AT LEAST NRAD) (INPUT)
C
C     THETA  - ANGULAR POSITION OF SURFACE POINTS
C                (DIMENSIONED AT LEAST NANG)
C
C     XP     - X-POSITION OF SURFACE POINTS
C                (DIMENSIONED AT LEAST NPOINT)
C
C     YP     - Y-POSITION OF SURFACE POINTS
C                (DIMENSIONED AT LEAST NPOINT)
C
C     X      - HORIZONTAL COORDINATE OF JET
C
C     Z      - VERTICAL COORDINATE OF JET
C
C     ZINC   - NON-DIMENSIONAL INCREMENTAL STEP SIZE FOR Z
C
C     DELTAZ - Z-POSITION OF EFFECTIVE/VIRTUAL SOURCE
C
C     DELDCK - EFFECTIVE BLOCKAGE CYLINDER DIAMETER
C
C     VKSAV  - CUMULATIVE VORTICITY ALONG THE JET
C
C     XI     - NATURAL COORDINATE TANGENT TO JET
C
C     ZETA   - NATURAL COORDINATE NORMAL TO JET
C
C     ETA    - NATURAL COORDINATE PERPENDICULAR TO XI
C                AND ZETA
C
C     ALPHA  - ANGLE BETWEEN X-AXIS AND XI-AXIS
C
C     DAREA  - INCREMENTAL PLATE AREA
```

```
C      TOTFOR - TOTAL RESULTANT FORCE ON PLATE
C      XBAR   - X-POSITION OF RESULTANT FORCE
C      VT     - NORMALIZED INDUCED FORCE
       IMPLICIT REAL*8 (A-H,O-Z)
       DIMENSION U(50,50),V(50,50),W(50,50),R(50),THETA(50),
      X          CP(50,50)
       DIMENSION XP(4500),YP(4500),ZP(4500)
C
C  DATA INPUT
C
       READ(2,60) NRAD
       READ(2,60) NANG
C   ZERO OUT STORAGE MATRICES
       NPOINT = NRAD*NANG
       DO 10 I = 1,NPOINT
       XP(I) = 0.0
       YP(I) = 0.0
       ZP(I) = 0.0
10     CONTINUE
       DO 30 I = 1,NRAD
       R(I) = 0.0
       DO 20 J = 1,NANG
       THETA(J) = 0.0
       U(I,J) = 0.0
       V(I,J) = 0.0
       CP(I,J) = 0.0
20     CONTINUE
30     CONTINUE
       READ(2,60) NTYPE
       READ(2,40) UJ,UM,D
       WRITE(6,50) UJ,UM,D
       READ(2,70) ZINC
       READ(2,70)(R(I),I=1,NRAD)
C   VELOCITY RATIO
       VR = UJ/UM
C   POSITION OF EFFECTIVE SOURCE
       DELTAZ = VR*DSQRT(VR)/15.0
C    CORRECTION FOR DELTAZ = 0.0
       IF(NTYPE.LE.1) DELTAZ = 0.001
       WRITE(6,80) DELTAZ
       WRITE(6,90) ZINC
40     FORMAT(3F8.4)
50     FORMAT('0',2X,'JET VELOCITY = ',F8.4,2X,'UNIFORM',
      X'VELOCITY = ',F8.4,2X,'JET DIAMETER = ',F8.4)
60     FORMAT(I4)
70     FORMAT(F10.5)
80     FORMAT('0',2X,'EFFECTIVE SOURCE IS',F5.2,2X,
      X'DIAMETERS ABOVE THE PLATE')
90     FORMAT ('0',2X,'Z STEP SIZE = ',F5.3)
C
C   DEFINITION OF PI
C
```

```
      PI = 2.0*ARSIN(1.00000000)
C
C   TRAJECTORY CONSTANT
C
      B = 0.19*VR**2
C
C  CALCULATION OF INTERFERENCE VELOCITY
C
      L = 0
      CALCON = DFLOAT(NANG) - 1.0
C   INCREMENT RADIUS (INPUT VALUES)
      DO 140 I = 1,NRAD
      RCALC = R(I)
C   INCREMENT THETA (5 DEGREE INCREMENTS)
      DO 130 J = 1,NANG
      K = J-1
      THETA(J) = DFLOAT(K)* (PI/CALCON)
C   SHIFT TO CARTESIAN COORDINATES
      L = L+1
      COST = DCOS(THETA(J))
      SINT = DSIN(THETA(J))
      XP(L) = RCALC*COST
      YP(L) = RCALC*SINT
C
      Z1 = 0.0
      Z2 = 0.00001
      THKSAV = 0.0
100   Z1 = Z2
      Z2 = Z1 + ZINC
      Z11 = Z1 + DELTAZ
      Z22 = Z2 + DELTAZ
      X1 = B*(DCOSH(Z1/B)-1.0)
      X2 = B*(DCOSH(Z2/B)-1.0)
      TANAB = (Z2-Z1)/(X2-X1)
      TANA1 = 1.0/DSINH(Z1/B)
      TANA2 = 1.0/DSINH(Z2/B)
      ALFONE = DATAN(TANA1)
      ALFTWO = DATAN(TANA2)
      ALFBAR = DATAN(TANAB)
      SINA1 = DSIN(ALFONE)
      SINA2 = DSIN(ALFTWO)
      SINAB = DSIN(ALFBAR)
      COSA1 = DCOS(ALFONE)
      COSA2 = DCOS(ALFTWO)
      COSAB = DCOS(ALFBAR)
C  NATURAL COORDINATES IN TERMS OF CARTESIAN COORDINATES
      XIONE = -(Z11*SINA1 + (X1-XP(L))*COSA1)
      XITWO = -(Z22*SINA2 + (X2-XP(L))*COSA2)
      XIBAR1 = -(Z11*SINAB + (X1-XP(L))*COSAB)
      XIBAR2 = -(Z22*SINAB + (X2-XP(L))*COSAB)
      ETA = YP(L)
      ZETA1 = (Z11*COSA1 - (X1-XP(L))*SINA1)
      ZETA2 = (Z22*COSA2 - (X2-XP(L))*SINA2)
      ZETAB = (Z11*COSAB - (X1-XP(L))*SINAB)
C
```

```
C  GEOMETRIC CONSTANTS
      ETPL = ETA + 0.5
      ETMI = ETA - 0.5
      SA = XICNE**2
      SB = XITWO**2
      SC = XIBAR1**2
      SD = XIBAR2**2
      SE = ZETA1**2
      SF = ZETA2**2
      SG = ZETAB**2
      SH = ETPL**2
      SI = ETMI**2
      CA = DSQRT(SA + SE + SH)
      CB = DSQRT(SA + SE + SI)
      CC = DSQRT(SB + SF + SH)
      CE = DSQRT(SB + SF + SI)
      CF = DSQRT(SD + SG + SI)
      CG = DSQRT(SC + SG + SI)
      CH = DSQRT(SD + SG + SH)
      CI = DSQRT(SC + SG + SH)

      CON1 = (ETPL/CA - ETMI/CB)/(SA + SE)
      CON2 = (ETPL/CC - ETMI/CE)/(SB + SF)
      CON3 = (XIBAR2/CF - XIBAR1/CG)/(SG + SI)
      CON4 = (XIBAR2/CH - XIBAR1/CI)/(SG + SH)

      U1 = ZETA1*CON1

      U2 = ZETA2*CON2

      V3 = ZETAB*CON3

      V4 = ZETAB*CON4

      W1 = XICNE*CON1

      W2 = XITWO*CON2

      W3 = ETMI*CON3

      W4 = ETPL*CON4

C  INCREMENTAL VORTICITY TERM

      FF = ((DEXP(Z2/B)-DEXP(Z1/B))/(1.0+DEXP((Z2+Z1)/B)))
C
      HK = (1.0/8.0)* VR**2 * DATAN(FF)

      HK = HK + HKSAV

      HKSAV = HK

C  INCREMENTAL INTERFERENCE VELOCITY COMPONENTS

      UP = 0.0
      UP = HK*((-W1*SINA1+W2*SINA2+(-W3+W4)*SINAB+U1*COSA1)
     X -(U2*COSA2))
C
      VP = 0.0
      VP =  HK*(V3 - V4)
C
C
      U(I,J) = U(I,J) + UP
      V(I,J) = V(I,J) + VP

C  TEST FOR CONVERGENCE

      TEST = DABS(UP) + DABS(VP)

      IF (TEST.LE.0.000001) GO TO 110
```

```
C
      GO TO 100
C
110   CONTINUE
C  CALCULATION OF BLOCKAGE VELOCITY TERM
      IF(NTYPE.EQ.0) GO TO 120
      IF(NTYPE.EQ.2) GO TO 120
C
      RBLOCK = 0.96/DSQRT(VR)
      DBLOCK = 2.0*RBLOCK*D
      RK = ((RBLOCK/R(I))**2)/2.0
      UC = RK*(SINT**2 - COST**2)
      VC = -2.0*RK*SINT*COST
      U(I,J) = U(I,J) + UC
      V(I,J) = V(I,J) + VC
C  CALCULATION OF PRESSURE COEFFICIENT
120    CP(I,J) = -4.0*(U(I,J) + U(I,J)**2 + V(I,J)**2)
C       CHANGE DESIGNATION OF VARIABLE
C
      ZP(L) = CP(I,J)
C
130   CONTINUE
140   CONTINUE
C  CALCULATION OF INCREMENTAL FORCE
      RO = 0.0
      RI = 0.0
      AREA = 0.0
      PAREA = 0.0
      FORCE = 0.0
      YMOM = 0.0
      TOTFOR = 0.0
      TYMOM = 0.0
      NAREA = NFAC - 1
      DO 170 I=1,NAREA
      K = I + 1
      RI = R(I)
      RO = R(K)
C  CALCULATION OF INCREMENTAL AREA
      AREA = PI*(RO**2 - RI**2)
      PAREA = AREA/(2.0*CALCON)
      DO 160 J=1,NANG
C  CALCULATION OF AVERAGE PRESSURE COEFFICIENT
      CPAVG = (CP(I,J) + CP(K,J))/2.0
C  CALCULATION OF EFFECTIVE FORCE
      FORCE = PAREA*CPAVG
      IF(..EQ.1) GO TO 150
      IF(J.EQ.NANG) GO TO 150
      FORCE = 2.0*FORCE
C  CALCULATION OF MOMENT ARM
```

```
150     XM = ((RC + RI)/2.0)*DCOS(THETA(J))
C   CALCULATION OF MOMENT ABOUT Y-AXIS
        YMOM = FORCE*XM
C   SUMMATION OF TOTAL FORCE
        TOTFOR = TOTFOR + FORCE
C   SUMMATION OF TOTAL MOMENT
        TYMOM = TYMOM + YMOM
160     CONTINUE
170     CONTINUE
C   CALCULATION OF CENTER OF ACTION
        XBAR = TYMOM/TOTFOR
C   CALCULATION OF NORMALIZED INDUCED FORCE: Y/T
        VRINV = 1.0/VR
        YT = 2.0*TOTFOR*VRINV**2/PI
C   DATA OUTPUT
        WRITE(6,260) DBLOCK
        WRITE(6,230) TOTFOR,XBAR
        WRITE(6,240) YT, VRINV
180     DO 220 I = 1,NANG
        ANGLE = THETA(I)*180.0/PI
        WRITE(6,190) ANGLE
190     FORMAT('0',2X,'THETA = ',F6.2,8X,'R',9X,'CP',9X,'U',
       X 9X,'V')
        DO 210 J = 1,NRAD
        WRITE(6,200) R(J),CP(J,I),U(J,I),V(J,I)
200     FORMAT(' ',23X,F6.2,2X,F8.2,3X,F6.2,4X,F6.2)
210     CONTINUE
220     CONTINUE
230     FORMAT('0',2X,'RESULTANT FORCE OF ',1X,F7.2,1X,
       X'ACTS AT X = ',F6.2)
240     FORMAT('0',2X,'Y/T = ',F6.2,1X,'FOR LM/UJ = ',F6.3)
        WRITE(7,250)(XP(I),YP(I),ZP(I),I=1,NPOINT)
250     FORMAT(3F20.4)
260     FORMAT('0',2X,'EFFECTIVE BLOCKAGE CYLINDER',
       X'DIAMETER = ',F4.2)
270     STOP
        END
```

LIST OF REFERENCES

1. English, J. W., "The Design and Performance of Lateral Thrust Units for Ships, Hydrodynamic Considerations," Trans. R.I.N.A., Vol. 105, 1963.

2. English, J. W., and Steele, B. N., "The Performance of Lateral Thrust Units for Ships as Affected by Forward Speed and Proximity of a Wall," Ship Division, N.P.L., Rep. No. 28, 1962.

3. Stuntz, G. R., and Taylor, R. J., "Some Aspects of Bow-Thruster Design," Trans. S.N.A.M.E., Vol. 72, 1964.

4. Chislett, M. S. and Bjorheden, O., "Influence of Ship Speed on the Effectiveness of a Lateral-Thrust Unit," Hydro-Og Aerodynamisk Laboratorium, Rep. No. Hy-8, April 1966.

5. Principles of Naval Architecture, S.N.A.M.E.

6. Bradbury, L. J. S. and Wood, M. N., "The Static Pressure Distribution Around A Circular Jet Exhausting Normally from a Plane Wall into an Airstream, C.P. No. 822, Brit. A.R.C., 1965.

7. Margason, R. J., "The Path of a Jet Directed at Large Angles to a Subsonic Free Stream," NASA TN D-4919, 1968.

8. Gordier, R. L., "Studies on Fluid Jets Discharging Normally into Moving Liquid," St. Anthony Falls Hyd. Lab., Tech. Paper, No. 28, Series B, Aug 1959.

9. Sucec, J. and Bowley, W. W., "Prediction of the Trajectory of a Turbulent Jet Injected into a Cross-flowing Stream," Journal of Fluids Engineering, Trans. A.S.M.E., Series I 98. Dec 1976.

10. Abramovich, G. N., The Theory of Turbulent Jets, MIT Press, 1963.

11. Jordinson, R., "Flow in a Jet Directed Normal to the Wind," R&M No. 3074, Brit. A.R.C., 1958.

12. Keffer, J. F. and Baines, W. D., "The Round Turbulent Jet a Crosswind," Journal of Fluid Mechanics, Vol. 15, 1963.

13. Volger, R. D., "Surface Pressure Distribution Induced on a Flat Plate by a Cold Air Jet Issuing Perpendicularly from the Plate and Normal to a Low-Speed Free-Stream Flow," NASA TN D-1629, 1963.

14. Fearn, R. L. and Weston, R. P., "Induced Pressure Distribution of a Jet in a Crossflow," NASA TN D-7916, 1975.

15. McMahon, H. M. and Mosher, K.D., "Experimental Investigation of Pressures Induced on a Flat Plate by a Jet Issuing into a Subsonic Crosswind," NASA SP-218.

16. Kamotani, Y. and Greber, I., "Experiments on a Turbulent Jet in a Crossflow," A.I.A.A. Journal, Dec 1974.

17. Wooler, P. T., Burghard, G. H. and Gallagher, J. T., "Pressure Distribution on a Rectangular Wing with a Jet Exhausting Normally into an Airstream," Journal of Aircraft, Vol. 4, 1967.

18. Wooler, P. T., "On the Flow Past a Circular Jet Exhausting at Right Angles from a Flat Plate or Wing," Journal of the Royal Aeronautical Soeiety, Vol. 71, March 1967.

19. Wu, J. C. and Wright, M. A., "A Blockage-Sink Representation of Jet Interference Effects for Noncircular Jet Orifices," NASA SP-218.

20. Adler, D. and Baron, A., "Prediction of a Three Dimensional Circular Turbulent Jet in Crossflow," Research Report, Israel Institute of Technology, Haifa, Israel, September 1978.

21. Schmitt, H., "Anderung einer Parallel stromung entlang einer ebenen Platte durch einen quer gerichteten Freistrahl," Zeitschrift fur Flugwissenschaften und Weltraum forschung, Sept/Oct 1979.

22. Durand, W.F., Aerodynamic Theory, Vol. II, SECT 1, Dover 1963.

23. Robertson, J. M., Hydrodynamics in Theory and Application, Prentice Hall Inc. 1965.

INITIAL DISTRIBUTION LIST

		No. Copies
1.	Defense Technical Information Center Cameron Station Alexandria, Virginia 22314	2
2.	Library, Code 0142 Naval Postgraduate School Monterey, California 93940	2
3.	Department Chairman, Code 69 Mx Department of Mechanical Engineering Naval Postgraduate School Monterey, California 93940	1
4.	Professor R.H. Nunn, Code 69 Nn Department of Mechanical Engineering Naval Postgraduate School Monterey, California 93940	5
5.	LCDR Bradford B. Waterman 468 Oak Street East Bridgewater, Massachusetts 02333	1